colonies were separated from dishes by using Cell Dissociation Solution (Sigma-Aldrich), and colonies (2×10^3) were replated on collagen-coated dishes. Cells were cultured in the induction medium (Supporting Table 2) for 14 days. Cloning rings were used to isolate total RNA of each colony. At least two separate experiments were performed, and more than five colonies were investigated.

GeneChip Analysis, RNA Isolation, and Real-Time Polymerase Chain Reaction. Details are shown in the Supplementary Methods.

Immunostaining. For detecting $CD44^+$ colonies, cells were fixed with cold absolute ethanol at 10 days after plating, and immunocytochemistry (ICC) for CD44 was carried out. Details of staining were previously reported.[15] The numbers of $CD44^+$ colonies at days 5 and 10 were counted, and positivity was calculated. Three separate experiments were performed. To measure the labeling index (LI), 40 μM of 5-bromo-2'-deoxyuridine (BrdU) were added to the medium 24 hours before fixation. In double ICC for CD44 and BrdU, a combination of the avidin-biotin peroxidase complex method (Vectastain ABC Elite Kit; Vector Laboratories Inc., Burlingame, CA) and the alkaline phosphatase method was used. For fluorescent immunohistochemistry, sliced liver samples were frozen using isopentane/liquid nitrogen, and materials were kept at 80°C until use. All Abs used for immunostaining are listed in Supporting Table 1. Sections were embedded with 90% glycerol including 0.01% *p*-phenylenediamine and 4,6-diamidino-2-phenylindole. A confocal laser microscope (Olympus, Tokyo, Japan) was used for observation, and findings were analyzed using DP Manager (Olympus).

Treatment With Fluorescein Diacetate. As previously reported,[20] fluorescein diacetate (FD; Sigma-Aldrich) was dissolved in dimethyl sulfoxide, and the solution was diluted with the culture medium. Then, 0.25% FD was added to the medium, and the dish was rinsed three times with warm PBS. Fluorescent images were immediately photographed using a phase-contrast microscope equipped with a fluorescence device (Olympus).

Enzyme Histochemisty for DPPIV. To identify donor cells, enzyme histochemistry for DPPIV was carried out. DPPIV enzyme activity was detected as previously described.[15] $DPPIV^+$ foci in livers were photographed using a microscope equipped with a CCD camera, and the area of each focus was measured using ImageJ software (http://rsb.info.nih.gov/ij/index.html).

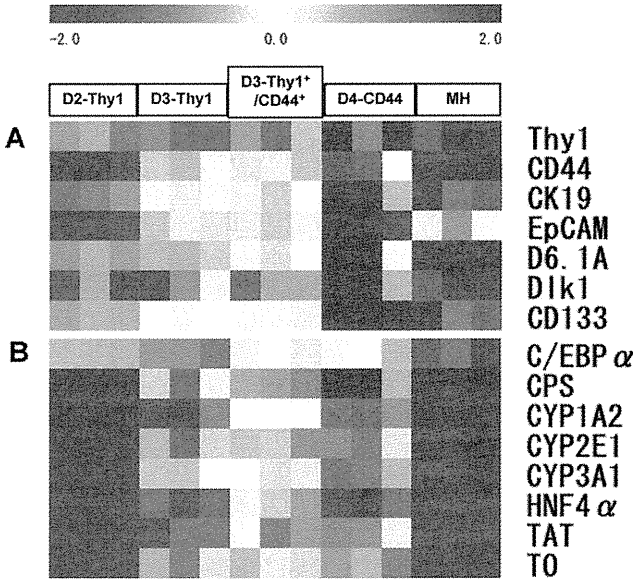

Fig. 1. Gene expression of sorted GalN-D2-$Thy1^+$ cells, D3-$Thy1^+$ cells, D3- $Thy1^+/CD44^+$ cells, and D4-$CD44^+$ cells. The gene-expression pattern of sorted cells was analyzed using GeneChip (Affymetrix, Inc., Santa Clara, CA). MHs isolated from a healthy adult rat liver were used as a control. A heatmap for genes that are classified into (A) stem cell and HPC markers and (B) hepatic markers. Relative expression of genes is shown in $\log_2$ scale. Increases in mRNA level are represented as shades of red and decreases as shades of blue.

Statistical Analysis. All data were analyzed using Turkey-Kramer's multiple comparison test. Level of statistical significance was $P < 0.05$. Experimental results are expressed as the geometric mean ± standard deviation.

Results

Characterization of Isolated Cells From Livers Treated by GalN. As previously reported,[15] $Thy1^+$ cells differentiated into hepatocytes through a $CD44^+$ intermediate state, as shown with clonally cultured $Thy1^+$ cells and cell transplantation. This transition likely happened in the GalN-treated rat liver as well. GeneChip data (Affymetrix, Inc., Santa Clara, CA) indicated that the immature hepatocyte markers, Dlk[21] and AFP were up-regulated in $Thy1^+CD44^+$ and Thy1 $CD44^+$ cells, whereas markers related to hepatic differentiation were gradually up-regulated during the transition from Thy1-D2 to CD44-D4 cells (Fig. 1). The results also suggested that most D2-$Thy1^+$ cells were not committed to the hepatic lineage. This is consistent with our previous finding that $Thy1^+$ cells isolated from GalN-D2 could form a few epithelial cell colonies in the standard medium for SH induction, whereas those from GalN-D3 certainly formed colonies consisting of $CD44^+$ cells. Therefore, we

Table 1. Effects of Growth Factors and Cytokines on the Formation of Epithelial Cell Colonies

Growth Factors	Numbers of Colonies/Well	Numbers of Cells/Colony
Control	0	0
EGF	4.5 ± 3.8	41.4 ± 1.8
bFGF	0.3 ± 0.6	13.0 ± 0.0
HGF	1.0 ± 1.7	24.6 ± 11.7
LIF	0	0
TNF α	0	0
IFN γ	0	0
OSM	0	0
PDGF BB	0	0
SCF	0	0
IL 6	0	0
TGF β1	0	0
TGF β2	0	0

Abbreviations: LIF, leukemia inhibitory factor; OSM, oncostatin M; PDGF BB, plate let derived growth factor BB; SCF, stem cell factor.

considered the possibility that Thy1$^+$ cells became the hepatocyte lineage between D2 and D3. To specify the factors that trigger hepatic commitment, we compared expression patterns of genes related to receptors of growth factors and cytokines and selected 12 candidates (Table 1).

Induction of Epithelial Cell Colonies by Growth Factors. D2-Thy1$^+$ cells were cultured in the medium supplemented with each factor. To elucidate the formation of epithelial cell colonies, ICC for CD44 was conducted 10 days after plating. Of the 12 candidates, only epidermal growth factor (EGF), basic fibroblast growth factor (bFGF), and hepatocyte growth factor (HGF) could induce colonies (Fig. 2A; Table 1). CD44 expression of cells varied among the colonies, and some colonies consisted of cells with low expression of CD44 (CD44 cells). Next, we examined whether bFGF and/or HGF could enhance the formation and expansion of colonies in the culture with EGF (Fig. 2B). Compared to EGF only (control), the addition of bFGF or HGF did not enhance the frequency of colony formation. In the combination of EGF and bFGF or HGF, the number of cells per colony increased to twice as many as in the control (Fig. 2C). In addition, the combination of the three factors also dose dependently increased the number of cells per colony. These results suggested that a certain number of Thy1$^+$ cells possessed the ability to differentiate into hepatic cells, and that the induction was initiated by EGF, bFGF, and/or HGF.

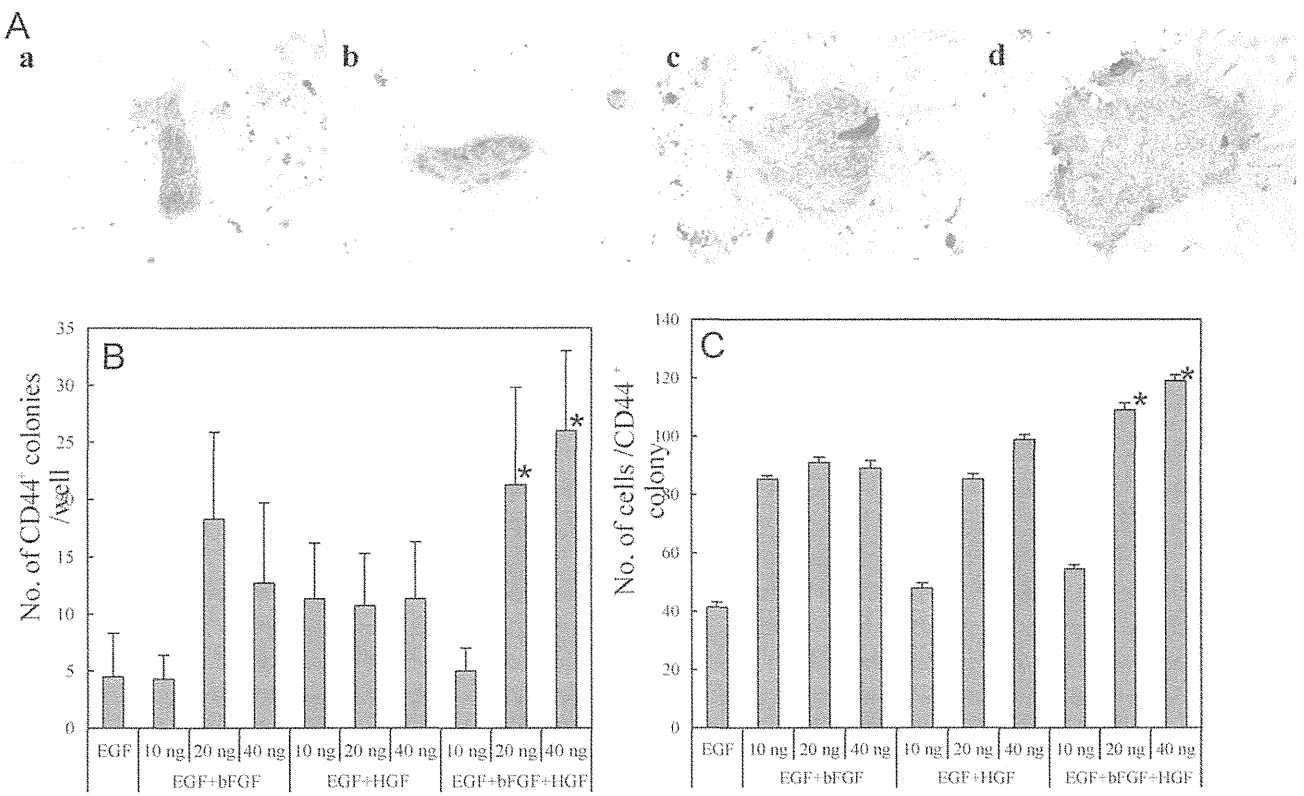

Fig. 2. Induction of CD44-positive cell colonies from sorted D2-Thy1$^+$ cells by treatment with EGF, bFGF, and/or HGF. Thy1$^+$ cells (1×10^5 viable cells/well) sorted from the GalN-D2 liver were plated on 12-well plates and cultured in medium supplemented with EGF (a), EGF+bFGF (b), EGF+HGF (c), and EGF+bFGF+HGF (d) for 10 days. Dose dependency of colony formation was examined. To identify colonies, ICC for CD44 was carried out. The number of CD44$^+$ cell colonies per well (B) and that of cells per colony (C) were measured. Asterisks shown in (B) and (C) indicate significance: $P < 0.05$, compared to EGF and 10 ng of EGF+bFGF+HGF.

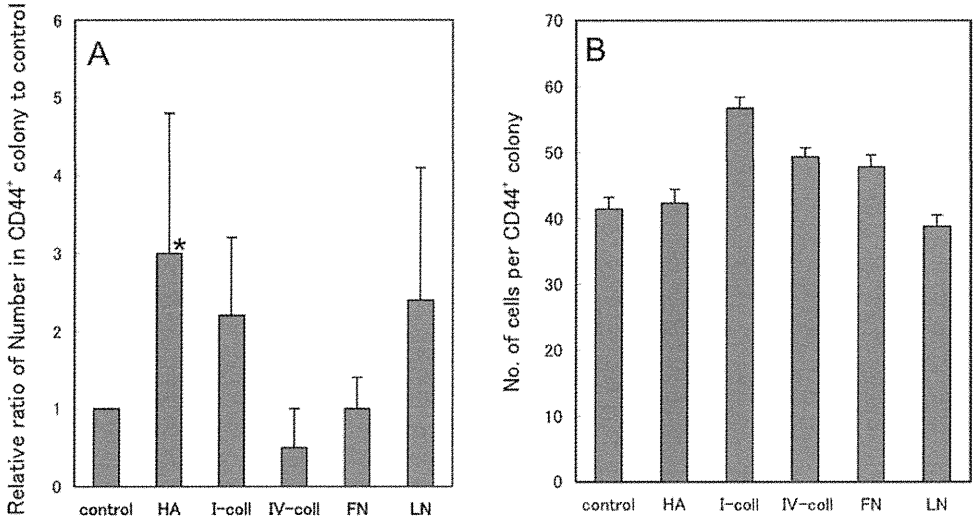

Fig. 3. Effects of ECM on colony formation of Thy1$^+$ cells were investigated. Thy1$^+$ cells were isolated from GalN-D2 rat livers and plated on dishes coated with hyaluronic acid (HA), type I collagen (I-coll), type IV collagen (IV-coll), fibronectin (FN), and laminin (LN). Noncoated dishes were used as controls. Cells were cultured in medium with EGF. To identify the colony, ICC for CD44 was carried out. The number of CD44$^+$ cell colonies per dish (A) and that of cells per colony (B) were measured. Asterisk shows significance: $P < 0.05$, control versus HA.

Induction of Epithelial Cell Colonies by Extracellular Matrix. Because CD44 is one of the receptors of hyaluronic acid (HA)[22,23] and because SHs can selectively proliferate on HA,[18] we investigated whether extracellular matrix (ECM) affected the frequency of emergence and phenotype of colonies derived from D2-Thy1$^+$ cells. Sorted D2-Thy1$^+$ cells were cultured on dishes coated with type I collagen, fibronectin, laminin, and HA, and ICC for CD44 was performed 10 days after plating. When cells were cultured in the medium supplemented with EGF, frequency of colony formation was significantly higher for cells on HA-coated dishes than for the control (Fig. 3A), but no difference was observed in the number of cells per colony among the dishes with each ECM (Fig. 3B).

Growth Ability and CD44 Expression of Cells Sorted From GalN-D3. Thy1$^+$CD44 (Thy1), Thy1$^+$CD44$^+$, and Thy1 CD44$^+$ (CD44) cells sorted from a GalN-D3 liver were cultured in the medium with EGF for 10 days. Double ICC for CD44 and BrdU was carried out (Fig. 4A–C). The frequency of colony formation was more than four times higher for CD44 cells than for both Thy1 and Thy1$^+$CD44$^+$ cells (Fig. 4D), and the average number of cells per colony was significantly larger for CD44 cells than for Thy1 and Thy1$^+$CD44$^+$ cells (Fig. 4E). The percentages of BrdU$^+$ cells were approximately 70% and 80% in colonies derived from Thy1 and CD44 cells, respectively (Fig. 4A–C, F). Growth ability of Thy1$^+$CD44$^+$ cells was also intermediate between those of Thy1 and CD44 cells.

Intensity and the localization of CD44 varied among cells forming colonies. In spite of the origin of sorted cells, CD44 protein was usually expressed in cell membranes between cells (Fig. 4C). Some colonies consisted of cells with CD44 protein localized in both the cell membrane and cytoplasm (Fig. 4A, B). The latter type of colony was often observed in the culture of Thy1 cells. CD44 positivity of Thy1$^+$ cells in a colony was approximately 65% at day 5 and increased to approximately 80% at day 10 (Fig. 4G).

Next, to examine whether acquisition of CD44 expression in Thy1$^+$ cells was also correlated to growth ability of cells *in vivo*, cell transplantation was carried out. D2-Thy1$^+$, D3-Thy1$^+$CD44$^-$, D3-Thy1$^+$CD44$^+$, D3-Thy1 CD44$^+$, and D4-CD44$^+$ cells (5×10^5 cells/rat) isolated from GalN-treated livers were intrasplenically transplanted into RET/PH-treated rats. One month after transplantation, the number of cells in foci derived from D4-CD44 was much larger than in those from Thy1-expressing cells (Fig. 4H, I). The growth rate of engrafted cells increased in correlation with the expression of CD44 and time after GalN treatment. In addition, no types of donor-derived (Y chromosome$^+$) cells, other than hepatocytes, could be found in recipient livers (Supporting Fig. 1).

Gene Expression of Hepatic Markers of Epithelial Cell Colonies Derived From D3-Thy1 Cells. To elucidate the characteristics of cells in colonies derived from D3-Thy1 cells, quantitative polymerase chain reaction (qPCR) of cells was performed for each colony, which was separated from the culture dish using a

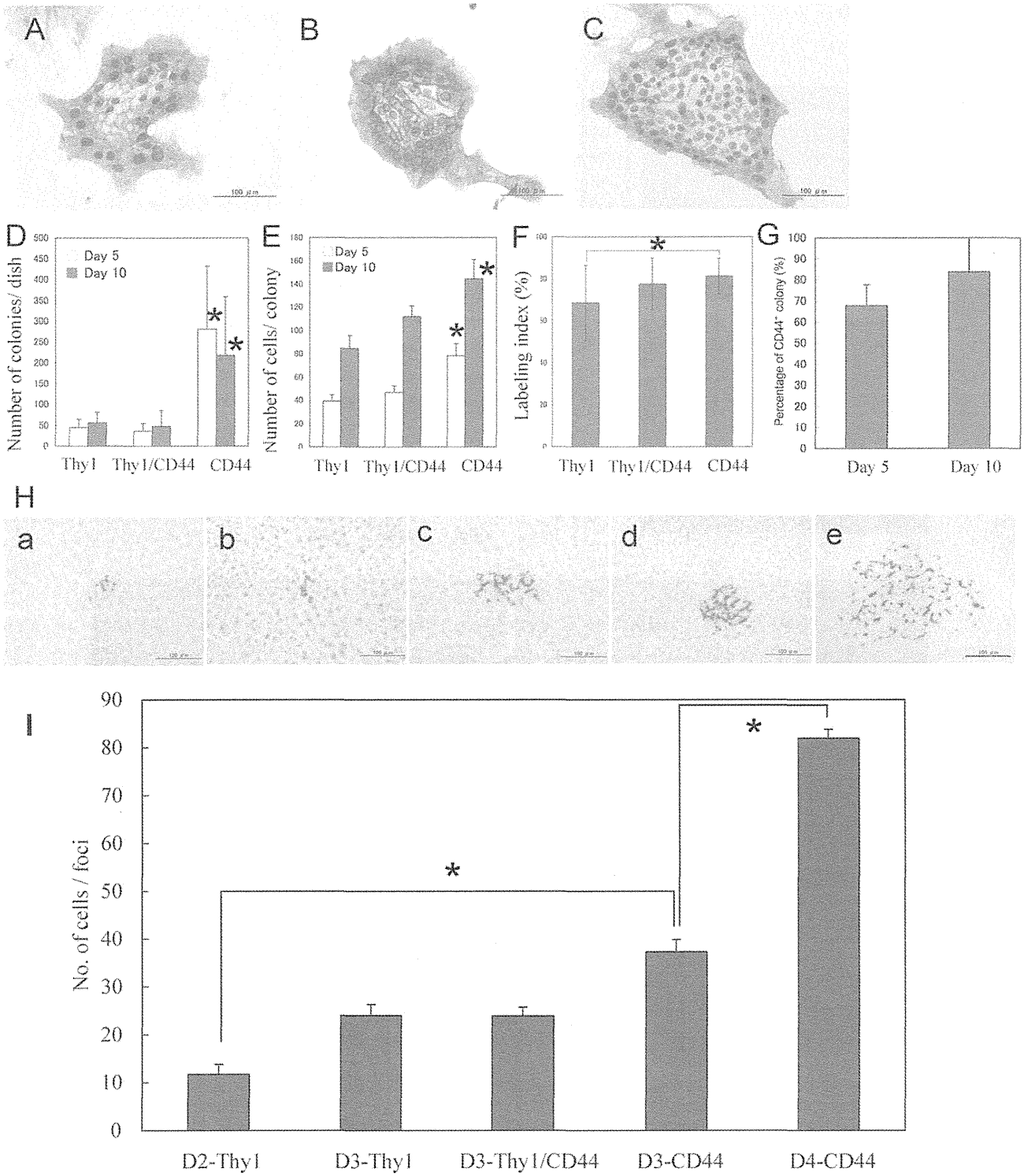

Fig. 4. Growth and CD44 positivity of epithelial cell colonies were examined in cultured cells. $Thy1^+$ (A), $Thy1^+/CD44^+$ (B), and $CD44^+$ cells (C) were isolated from GalN-D3 rat livers. Then, viable cells per dish (1×10^5) were plated on noncoated 35-mm culture dishes and cultured in the medium with EGF for 10 days. BrdU (40 μmol/L) was added to the medium 24 hours before fixation. At 5 and 10 days after plating, cells were fixed and double ICC for CD44 and BrdU was performed. CD44 and BrdU were stained violet and brown, respectively. Nuclei were counterstained with hematoxylin. The number of $CD44^+$ colony per dish (D), cells per colony (E), $BrdU^+$ cells per colony (F), and CD44 positivity of the colony derived from D2-$Thy1^+$ cells (G) were measured at 5 (white bar) and 10 days (gray bar) after plating. $CD44^+$ cell colonies were defined as colonies in which more than 90% of cells were stained with CD44. Asterisks show significant differences: $P < 0.05$. (D) $Thy1^+CD44^-$ and $Thy1^+CD44^+$ versus $Thy1^-CD44^+$ at days 5 and 10, (E) $Thy1^+CD44^-$ and $Thy1^+CD44^+$ versus $Thy1^-CD44^+$ at day 5, and $Thy1^+CD44^-$ versus $Thy1^-CD44^+$ at day 10, (F) $Thy1^+CD44^-$ versus $Thy1^-CD44^+$. Transplantation of isolated cells from GalN-treated livers into RET/PH-treated livers (H). Sorted GalN-D2-$Thy1^+$ (5×10^5 cells) (a), D3-$Thy1^+/CD44^-$ (b), D3-$Thy1^+/CD44^+$ (c), D3-$Thy1^-/CD44^+$ (d), or D4-$CD44^+$ cells (e) were intrasplenically transplanted into Ret/PH-treated rats. Thirty days after transplantation, livers were perfused with PBS, then sliced to make frozen sections. Tissues were enzymatically stained with DPPIV. DPPIV-positive cells are stained red. Nuclei are counterstained with hematoxylin (blue). The number of cells per focus was measured (I). Asterisks indicate significant differences: $P < 0.05$.

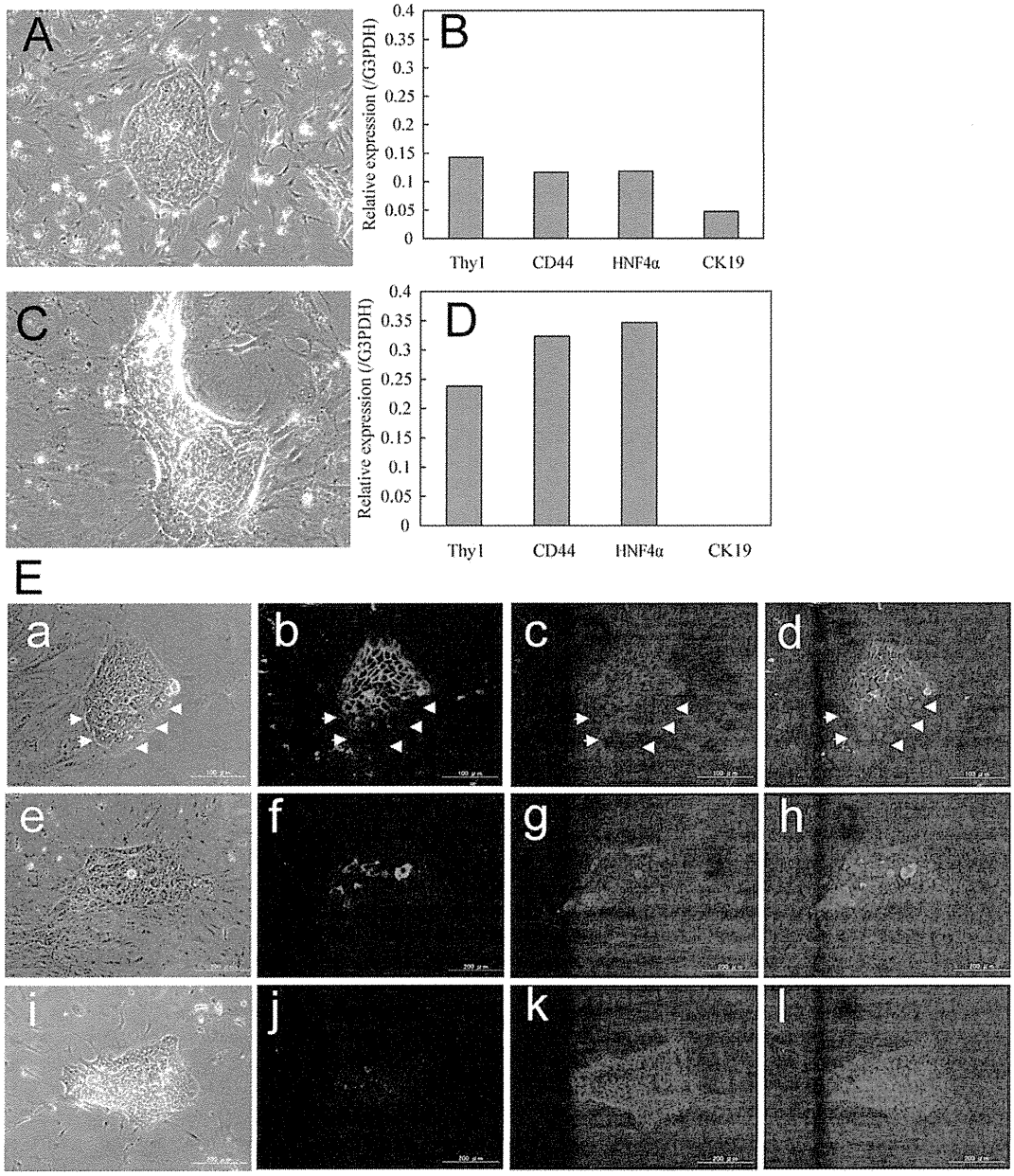

Fig. 5. Gene expression of the cells in each colony was measured by qPCR. Thy1^{+} cells sorted from GalN-D3 livers were cultured in the medium with EGF for 10 days. Each colony was separated from the dishes by using a cloning ring. Phase-contrast photos of all colonies were taken, then RNA of cells in the colonies was separated. qPCR was performed for each colony. Morphology (A and C) and gene expression (B and D) of representative colonies of CD44^{low} (A and B) and CD44^{high} (C and D) are shown. Cells were fixed at day 10, and double ICC for CD44/Thy1 (E, a-d) and CK-19/Alb (E, e-l) was performed. Although many cells in Thy1-derived colonies coexpressed CD44 and Thy1, some large cells (arrowheads) exhibited no expression of either protein (E, a-d). There were some colonies consisting of a mixture of Alb^{+} and CK-19^{+} cells (E, e-h), but most cells expressed Alb and only a few cells expressed CK-19 (E, i-l). Data for other colonies are shown in Supporting Fig. 2.

cloning ring. Phase-contrast photos were taken of every colony, and qPCR was performed. Gene-expression patterns of the colonies were roughly divided into two groups by the level of CD44 expression. Results for a representative colony in each group are shown in Fig. 5 (results for other colonies are shown in Supporting Fig. 2). Although intensity of gene expression varied among colonies, all colonies expressed CD44 messenger RNA (mRNA). Compared to cells in CD44^{low} colonies, those in CD44^{high} colonies showed not only relatively high expression of albumin and hepatocyte nuclear factor (HNF)-4α, but also suppression of CK-19 expression. Although coexpression of CD44 and Thy1 was observed in many Thy1-derived colonies, some large cells (arrowheads) exhibited no expression of either protein (Fig. 5E, a–d). There were colonies consisting of a mixture of albumin (Alb)$^{+}$ and CK-19^{+} cells (Fig. 5E, e–h), though most cells expressed

Alb and only a few cells exhibited CK-19 (Fig. 5E, i–l). To induce maturation of cells in Thy1-derived colonies, cells were treated with Matrigel. The treatment dramatically decreased Thy1 expression and increased levels of both HNF-4α and Alb (Supporting Fig. 3A). In addition, a marked increase of Alb secretion was also observed in cells with Matrigel (Supporting Fig. 3B). However, neither CD44 nor CK-19 expression was changed by the treatment.

Induction of Maturation in Cultured Cells. Next, we examined whether the newly generated hepatocytes could reconstruct hepatic organoids with highly differentiated functions. To enhance the organoid formation of colonies, colonies derived from D3-Thy1, CD44, and SHs from a healthy liver were replated on collagen-coated dishes to increase their density. In contrast to the Matrigel treatment, this procedure resulted in natural organoid formation, which consisted of piled-up cells with BCs. The expression of CCAAT/enhancer-binding protein (C/EBP)-α was ICC examined, and expression of genes related to hepatic differentiated functions was investigated by qPCR. In addition, to certify the function of the newly formed BCs, FD was added to the culture medium and the ability to secrete fluorescence into BCs was examined.

In spite of their origins, some cells in colonies became large and piled up with time after replating. Morphologically, BCs and cyst-like structures were observed in colonies, similar to those in colonies formed by SHs derived from healthy rat liver.[13,19,20] However, ICC for C/EBP-α revealed that the numbers of positive nuclei in Thy1- and CD44-derived colonies were smaller than in SH-derived colonies (Figs. 6A, B). Results of qPCR for each colony derived from Thy1, CD44, and SHs revealed that gene expression of cytochrome P450 1A2 (CYP1A2), tryptophan 2,3-dioxygenase (TDO), and carbamoylphosphate synthetase I (CPS-I), which are regarded as indicators for differentiated hepatic functions, was significantly higher in SH than CD44 or Thy1 (Fig. 6C). However, expression of tyrosine aminotransferase (TAT) was not different among cells.

In a SH-derived colony, fluorescence was secreted into BCs and accumulated in cysts (Fig. 7, e,f). The networks of BCs were well developed, corresponding to the regions of piled-up cells. On the other hand, in the colonies derived from both Thy1 (Fig. 7A, a,b) and CD44 cells (Figs. 7A, c,d), part of the region consisting of piled-up cells had a green, patch-like appearance. This phenomenon indicated the retention of fluorescence in the cytoplasm. In addition, to quantitatively compare structural differentiation among cells, the total length of BCs was measured in each colony. Total length of BCs was significantly larger in the SH-derived colony than in the Thy1- and CD44-derived colonies (Fig. 7B). These results suggested that newly generated hepatocytes derived from Thy1 and CD44 were not as mature as those from SHs.

Discussion

Hepatocytic Differentiation of Thy1-Positive Cells. Thy1 was first identified as a marker of oval cells by Petersen et al.[24] and then widely used in experiments with HPCs. Recently, a question was raised about the validity of Thy1 as a marker for oval cells.[25,26] It was reported that Thy1 was not a marker of oval cells, but of hepatic myofibroblasts and/or stellate cells. Although the issue regarding whether Thy1 is a marker for hepatic stem/progenitors is open to debate, we recently found that some $Thy1^+$ cells isolated from GalN-treated livers differentiated into $CD44^+$ hepatocytes through $Thy1^+CD44^+$ cells.[15] These results suggested that the population of $Thy1^+$ cells was heterogeneous, and that it contained putative hepatic stem cells possessing the ability to differentiate into hepatocytes. Interestingly, colony formation was clearly observed in the culture of cells from GalN-D3, whereas it was rarely observed in $Thy1^+$ cells isolated from GalN-D2, suggesting that $Thy1^+$ cells became the hepatic lineage between D2 and D3. In the present experiment, we demonstrated that EGF, fibroblast growth factor (FGF), and HGF might trigger the commitment to the hepatic lineage of $Thy1^+$ cells, some of which possess capability as putative stem cells. It has been reported that transforming growth factor (TGF)-α, HGF, and FGF play important roles in stem/progenitor cell-mediated liver regeneration. Indeed, the growth factors are transcriptionally upregulated during the period of active proliferation and differentiation of progenitor cells in rat liver[27–29] and appear to drive the early proliferation of the progenitor cell compartment.[27,30] Interestingly, it has been reported that stellate cells, which proliferate concomitantly and in close contact with progenitor cells,[31] appear to be the main source of TGF-α, HGF, and acidic FGF, whereas the corresponding cognate receptors are strongly expressed in progenitor cells, suggesting that the regulation of progenitor cell proliferation and differentiation by growth factors occurs primarily in a paracrine manner.[2,5] On the other hand, it is well known that priming factors are necessary for the emergence and proliferation of HPCs.[5,7] A correlation between the severity of liver disease and the magnitude

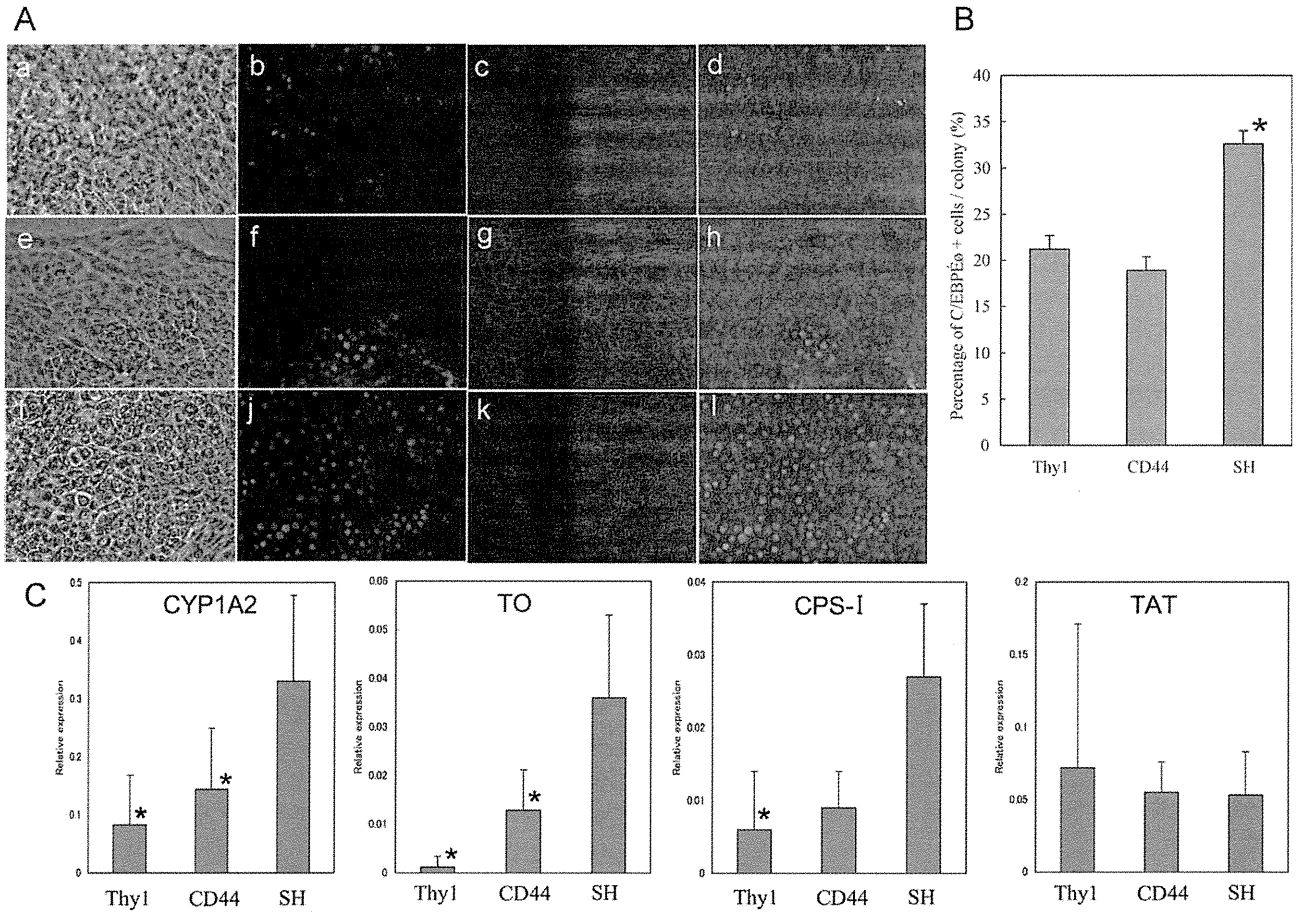

Fig. 6. To enhance organoid formation of the colonies, colonies derived from GalN-D3 Thy1 cells (A, a-d), CD44 cells (A, e-h), and a healthy liver (A, i-l) were replated on new collagen-coated dishes at 10 days after plating to increase the density of the colonies. Cells were cultured for more than 14 days after replating. This procedure resulted in natural organoid formation, which consisted of piled-up (matured) cells. The expression of C/EBP-α (A,b,f,j) and CD44 (A,c,g,k) was ICC observed and the percentage of C/EBP-α^+ cells per colony was measured (B). The gene expression of CYP1A2, TDO, CPS-I, and TAT in Thy1, CD44 cells, and SHs derived from a healthy liver was analyzed by real-time PCR (C). The scale is shown as a value relative to that of MH. Asterisks indicate a significant difference: $P < 0.05$, SH versus Thy1 or CD44.

of the response of hepatic progenitor cells has been reported and inflammatory cytokines, such as tumor necrosis factor alpha (TNF-α), interleukin (IL)-6, and interferon-gamma (INF-γ), were suggested to play central roles as priming factors in rodents.[32–36] However, in the present experiment, TNF-α, IL-6, and INF-γ could not induce the epithelial differentiation of Thy1$^+$ cells or enhance their expansion. This might be because D2-Thy1$^+$ cells have already been primed by the inflammation induced by GalN.

Expression of CD44 in Thy1-Derived Cells. In this experiment, we demonstrated that the growth and degree of hepatocytic differentiation of Thy1$^+$ cells were correlated with the expression of CD44. The results of GeneChip analysis demonstrated that the expression of genes related to hepatocytic differentiation, which were absent in GalN-D2-Thy1 cells, progressively increased in the order D3-Thy1, D3-Thy1$^+$CD44$^+$, and D4-CD44 cells. Although results of qPCR showed that the degree of expression of the genes of interest was different among epithelial colonies derived from D3-Thy1 cells, the cells in the CD44^{high} colonies showed high expression of Alb and HNF-4α, compared to cells in CD44^{low} colonies. In fact, CD44 expression in Thy1$^+$ cells increased with time in culture.

Acquisition of CD44 expression in Thy1$^+$ cells was also correlated with growth ability of cells. Growth of cells in CD44$^+$ cell-derived colonies was clearly faster than that of cells in colonies derived from Thy1-expressing cells. High growth activity of CD44$^+$ cells was also shown in the cell transplantation experiment. One month after transplantation, the number of cells in the foci derived from D4-CD44 was much larger than in those from Thy1-expressing cells. In general, the growth speed of cells shows an inverse correlation with degree of cell differentiation, and less-differentiated cells can proliferate much faster than differentiated cells. However, in the present experiment, although

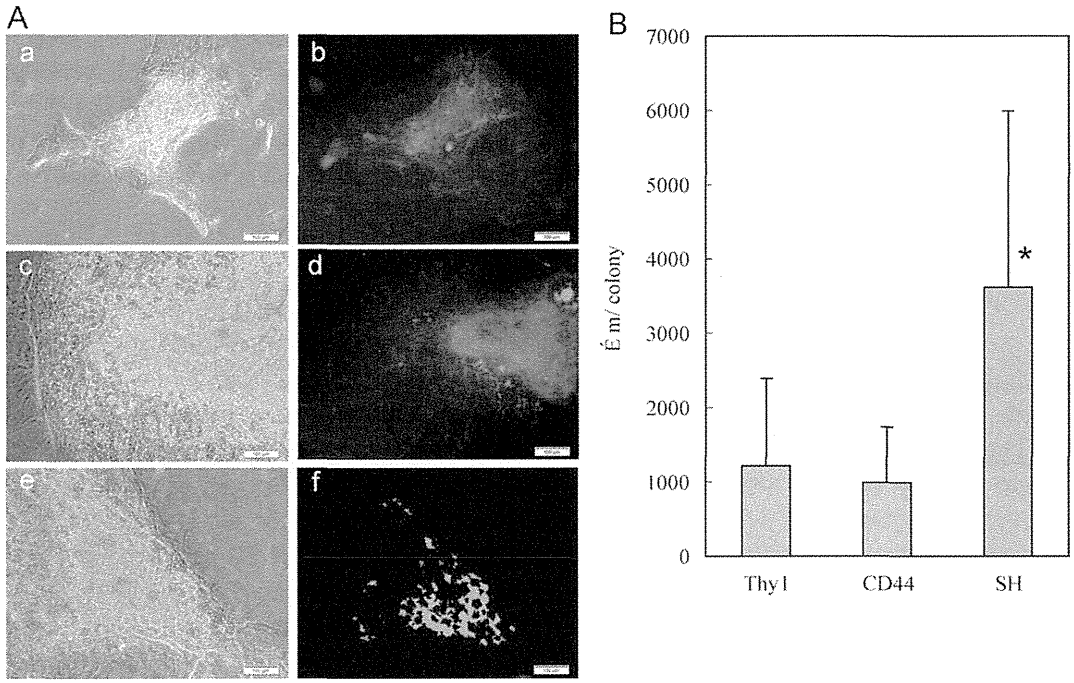

Fig. 7. To demonstrate the function of the newly formed BCs in hepatic organoids, FD was added to the culture medium and the ability to secrete fluorescence into BCs was examined. A part of the region consisting of piled-up cells in the colonies derived from both Thy1 (A, a,b) and CD44 cells (A, c,d) shows a green, patch-like appearance. Fluorescence was secreted into BCs and accumulated in the cysts in an SH-derived colony. To compare the development of BCs, the total length of BCs was measured in each colony (B). Total length of BCs was significantly larger in the SH-derived colony than in the Thy1- and CD44-derived colonies. Asterisk indicates a significant difference: $P < 0.05$, SH versus Thy1 and CD44.

$CD44^+$ cells were more differentiated than $Thy1^+$ cells, growth speed of $CD44^+$ cells was higher than that of CD44 cells (data not shown). At present, we cannot explain these findings, and further experiments will be required to clarify the regulatory mechanism of CD44 expression.

Restricted Maturation of HPCs. We previously reported that SHs derived from the healthy liver could spontaneously differentiate into hepatocytes that showed typical features of MHs and reconstructed three-dimensional (3D) structures by interacting with hepatic nonparenchymal cells.[11] In 3D structures, a complicated network of BCs is formed, and, when FD is added, fluorescence is secreted to BCs and expands all over the colony.[11,20] In the present experiment, despite their origins, cells could become large and pile up to form 3D structures that were morphologically similar to the hepatic organoids previously reported.[11,13] However, fluorescence was mostly retained in the cytoplasm of cells derived from both $Thy1^+$ and $CD44^+$ cells. Cytoplasmic retention of fluorescence indicates that cellular polarity is not well established, so that BCs cannot be well reconstructed. The short length of BCs also showed the incomplete maturation of both Thy1- and CD44-derived cells. Furthermore, compared to the organoids derived from SHs, CD44 expression remained and the ratio of C/EBP-α^+ cells was lower in organoids derived from both $Thy1^+$ and $CD44^+$ cells. The lower expression of CYP1A2, TDO, and CPS-I genes in organoids from Thy1 and CD44 than in those from SHs also indicated the immaturity of stem/progenitor cell-derived hepatocytes. These results demonstrated that the newly generated hepatocytes derived from $Thy1^+$ and $CD44^+$ cells might not have acquired the same highly differentiated functions as MHs. On the other hand, we previously reported that, compared to MHs, the repopulation efficiency of the liver by transplanted $Thy1^+$ cells was very low, and that most Thy1-derived foci disappeared within 2 months after transplantation.[16] Similar results were shown for the transplantation of $CD44^+$ cells. Those results indicate that HPCs may not be able to survive for a long time. Detailed histological analysis at 2 weeks after transplantation revealed that the percentage of C/EBP-α^+ cells in the early CD44-derived foci was lower than that in MH-derived foci. In addition, the size and shape of the cells and the distribution of the $DPPIV^+$ membrane were more irregular in Thy1- and CD44-derived foci than in MH-derived foci, which meant that BCs were not connected among cells, and that sinusoids were indistinct.[16] These cell-transplantation results may reflect the *in vitro* data shown in the present experiments. Shafritz et al.[6] summarized previous transplantation experiments using HPCs, and found that cells showed very low efficiency

of engraftment and repopulation, regardless of the condition of the recipient liver. Thus, hepatocytes induced from embryonic stem cells and other stem/progenitor cells have not yet matured to the stage at which they can efficiently repopulate the liver of an adult. In other words, to use HPCs in regenerative medicine, the state of differentiation of the cells used for cell transplantation may be very important, and a procedure for assessment of the maturation should be immediately developed.

Acknowledgments: The authors thank Ms. Minako Kuwano and Ms. Yumiko Tsukamoto for their technical assistance. The authors also thank Mr. Kim Barrymore for his help with the manuscript for this article.

References

1. Sell S. Heterogeneity and plasticity of hepatocyte lineage cells. HEPATOLOGY 2001;33:738-750.
2. Fausto N. Liver regeneration and repair: hepatocytes, progenitor cells, and stem cells. HEPATOLOGY 2004;39:1477-1487.
3. Michalopoulos GK. Liver regeneration: alternative epithelial pathways. Int J Biochem Cell Biol 2011;43:173-179.
4. Farber E. Similarities in the sequence of early histological changes induced in the liver of the rat by ethionine, 2-acetylaminofluorene, and 3'-methy-4-dimethylaminoazobenzene. Cancer Res 1956;16:142-149.
5. Santoni-Rugiu E, Jelnes P, Thorgeirsson SS, Bisgaard HC. Progenitor cells in liver regeneration: molecular responses controlling their activation and expansion. APMIS 2005;113:876-902.
6. Shafritz DA, Oertel M, Menthena A, Nierhoff D, Dabeva MD. Liver stem cells and prospects for liver reconstitution by transplanted cells. HEPATOLOGY 2006;43:S89-S98.
7. Bird TG, Lorenzini S, Forbes SJ. Activation of stem cells in hepatic diseases. Cell Tissue Res 2008;331:283-300.
8. Lemire JM, Shiojiri N, Fausto N. Oval cell proliferation and the origin of small hepatocytes in liver injury induced by D-galactosamine. Am J Pathol 1991;139:535-552.
9. Evarts RP, Hu Z, Omori N, Omori M, Marsden ER, Thorgeirsson SS. Precursor-product relationship between oval cells and hepatocytes: comparison between tritiated thymidine and bromodeoxyuridine as tracers. Carcinogenesis 1996;17:2143-2151.
10. Mitaka T, Kojima T, Mizuguchi T, Mochizuki Y. Growth and maturation of small hepatocytes isolated from adult liver. Biochem Biophys Res Commun 1995;214:310-317.
11. Mitaka T, Sato F, Mizuguchi T, Yokono T, Mochizuki Y. Reconstruction of hepatic organoid by rat small hepatocytes and hepatic nonparenchymal cells. HEPATOLOGY 1999;29:111-125.
12. Sasaki K, Kon J, Mizuguchi T, Chen Q, Ooe H, Oshima H, et al. Proliferation of hepatocyte progenitor cells isolated from adult human livers in serum-free medium. Cell Transplant 2008;17:1221-1230.
13. Sugimoto S, Mitaka T, Ikeda S, Harada K, Ikai I, Yamaoka Y, et al. Morphological changes induced by extracellular matrix are correlated with maturation of rat small hepatocytes. J Cell Biochem 2002;87: 16-28.
14. Kon J, Ooe H, Oshima H, Kikkawa Y, Mitaka T. Expression of CD44 in rat hepatic progenitor cells. J Hepatol 2006;45:90-98.
15. Kon J, Ichinohe N, Ooe H Chen Q, Sasaki K, Mitaka T. Thy1-positive cells have bipotential ability to differentiate into hepatocytes and biliary epithelial cells in galactosamine-induced rat liver regeneration. Am J Pathol 2009;175:2362-2371.
16. Ichinohe N, Kon J, Sasaki K, Nakamura Y, Ooe H, Tanimizu N, et al. Growth ability and repopulation efficiency of transplanted hepatic stem, progenitor cells, and mature hepatocytes in retrorsine-treated rat livers. Cell Transplant 2012;21:11-22.
17. Gordon GJ, Coleman WB, Grisham JW. Temporal analysis of hepatocyte differentiation by small hepatocyte-like progenitor cells during liver regeneration in retrorsine-exposed rats. Am J Pathol 2000;157:771-786.
18. Chen Q, Kon J, Ooe H, Sasaki K, Mitaka T. Selective proliferation of rat hepatocyte progenitor cells in serum-free culture. Nat Protoc 2007; 2:1197-1205.
19. Oshima H, Kon J, Ooe H, Hirata K, Mitaka T. Functional expression of organic anion transporters in hepatic organoids reconstructed by rat small hepatocytes. J Cell Biochem 2008;104:68-81.
20. Sudo R, Ikeda S, Sugimoto S, Harada K, Hirata K, Tanishita K, et al. Bile canalicular formation in hepatic organoid reconstructed by rat small hepatocytes and nonparenchymal cells. J Cell Physiol 2004;199: 252-261.
21. Tanimizu N, Nishikawa M, Saito H, Tsujimura T, Miyajima A. Isolation of hepatoblasts based on the expression of Dlk/Pref-1. J Cell Sci 2003;116:1775-1786.
22. Goodison S, Urquidi V, Tarin D. CD44 cell adhesion molecules. Mol Pathol 1999;52:189-196.
23. Ponta H, Sherman L, Herrlich PA. CD44: from adhesion molecules to signalling regulators. Nat Rev Mol Cell Biol 2003;4:33-45.
24. Petersen BE, Goff JP, Greenberger JS, Michalopoulos GK. Hepatic oval cells express the hematopoietic stem cell marker Thy-1 in the rat. HEPATOLOGY 1998;27:433-445.
25. Dezső K, Jelnes P, László V, Baghy K, Bödör C, Paku S, et al. Thy-1 is expressed in hepatic myofibroblasts and not oval cells in stem cell-mediated liver regeneration. Am J Pathol 2007;171:1529-1537.
26. Dudas J, Mansuroglu T, Batusic D, Saile B, Ramadori G. Thy-1 is an *in vivo* and *in vitro* marker of liver myofibroblasts. Cell Tissue Res 2007;329:503-514.
27. Evarts RP, Hu Z, Fujio K, Marsden ER, Thorgeirsson SS. Activation of hepatic stem cell compartment in the rat: role of transforming growth factor α, hepatocyte growth factor, and acidic fibroblast growth factor in early proliferation. Cell Growth Differ 1993;4:555-561.
28. Marsden ER, Hu Z, Fujio K, Nakatsukasa H, Thorgeirsson SS, Evarts RP. Expression of acidic fibroblast growth factor in regenerating liver and during hepatic differentiation. Lab Invest 1992;67:427-433.
29. Hu Z, Evarts RP, Fujio K, Omori N, Omori M, Marsden ER, et al. Expression of transforming growth factor alpha/epidermal growth factor receptor, hepatocyte growth factor/c-*met*, and acidic fibroblast growth factor/fibroblast growth factor receptors during hepatocarcinogenesis. Carcinogenesis 1996;17:931-938.
30. Nagy P, Bisgaard HC, Santoni-Rugiu E, Thorgeirsson SS. *In vivo* infusion of growth factors enhances the mitogenic response of rat hepatic ductal (oval) cells after administration of 2-acetylaminofluorene. HEPATOLOGY 1996;23:71-79.
31. Paku S, Schnur J, Nagy P, Thorgeirsson SS. Origin and structural evolution of the early proliferating oval cells in rat liver. Am J Pathol 2001;158:1313-1323.
32. Nagy P, Kiss A, Schnur J, Thorgeirsson SS. Dexamethasone inhibits the proliferation of hepatocytes and oval cells but not bile duct cells in rat liver. HEPATOLOGY 1998;28:423-429.
33. Bisgaard HC, Müller S, Nagy P, Rasmussen LJ, Thorgeirsson SS. Modulation of the gene network connected to interferon-γ in liver regeneration from oval cells. Am J Pathol 1999;155:1075-1085.
34. Knight B, Yeoh GC, Husk KL, Ly T, Abraham LJ, Yu C, et al. Impaired preneoplastic changes and liver tumor formation in tumor necrosis factor receptor type 1 knockout mice. J Exp Med 2000;192: 1809-1818.
35. Knight B, Matthews VB, Akhurst B, Croager EJ, Klinken E, Abraham LJ, et al. Liver inflammation and cytokine production, but not acute phase protein synthesis, accompany the adult liver progenitor (oval) cell response to chronic liver injury. Immunol Cell Biol 2005;83:364-374.
36. Matthews VB, Klinken E, Yeoh GC. Direct effects of interleukin-6 on liver progenitor oval cells in culture. Wound Repair Regen 2004;12: 650-656.

Zoledronic Acid But Not Somatostatin Analogs Exerts Anti-Tumor Effects in a Model of Murine Prostatic Neuroendocrine Carcinoma of the Development of Castration-Resistant Prostate Cancer

Kohei Hashimoto,[1] Naoya Masumori,[1]* Toshiaki Tanaka,[1] Toshihiro Maeda,[1] Ko Kobayashi,[1] Hiroshi Kitamura,[1] Koichi Hirata,[2] and Taiji Tsukamoto[1]

[1]Department of Urology, Sapporo Medical University School of Medicine, Japan
[2]First Department of Surgery, Sapporo Medical University School of Medicine, Japan

BACKGROUND. Since neuroendocrine (NE) cells play an important role in the development of castration-resistant prostate cancer (CRPC), target therapy to NE cells should be considered for treating CRPC. We investigated the effects zoledronic acid (ZOL) and two somatostatin analogs (octreotide: SMS, and pasireotide: SOM) on an NE allograft (NE-10) and its cell line (NE-CS), which were established from the prostate of the LPB-Tag 12T-10 transgenic mouse.

METHODS. We examined the in vivo effects of ZOL, SMS and SOM as single agents and their combinations on subcutaneously inoculated NE-10 allografts and the in vitro effects on NE-CS cells. Apoptosis and cell cycle activity were assessed by immunohistochemistry using TdT-mediated dUTP-biotin nick-end labeling (TUNEL) and a Ki-67 antibody, respectively.

RESULTS. In vivo growth of NE-10 tumors treated with ZOL, ZOL plus SMS, or ZOL plus SOM was significantly inhibited compared to the control as a consequence of induction of apoptosis and cell cycle arrest. ZOL induced time- and dose-dependent inhibition of in vitro proliferation of NE-CS cells, but the somatostatin analogs (SMS and SOM) did not. ZOL also inhibited migration of NE-CS cells. These effects were caused by inhibition of Erk1/2 phosphorylation via impairment of prenylation of Ras.

CONCLUSIONS. ZOL, but not SMS or SOM, induced apoptosis and inhibition of proliferation and migration through impaired prenylation of Ras in NE carcinoma models. Our findings support the possibility that ZOL could be used in the early phase for controlling NE cells, which may trigger progression to CRPC. *Prostate 73: 500 511, 2013.*

KEY WORDS: **zoledronic acid; somatostatin analog; neuroendocrine carcinoma; prostate cancer; anti-tumor effect**

INTRODUCTION

Prostate cancer is the most common noncutaneus malignancy in men in developed countries [1]. Its incidence has been gradually increasing even in non-Caucasian men. As the growth of cancer cells is androgen-dependent, androgen deprivation therapy including surgical or chemical castration has been the mainstay of treatment for advanced prostate cancer. The response to this treatment lasts for a median of 36–48 months [2]. However, in most cases, the disease progresses despite the castration level of serum testosterone, and results in castration-resistant prostate cancer (CRPC). The prognosis of CRPC is poor and a concrete treatment strategy has not yet been established.

*Correspondence to: Naoya Masumori, Department of Urology, Sapporo Medical University School of Medicine S1, W16, Chuo ku, Sapporo 060 8543, Japan. E mail: masumori@sapmed.ac.jp
Received 4 June 2012; Accepted 27 August 2012
DOI 10.1002/pros.22590
Published online 19 September 2012 in Wiley Online Library (wileyonlinelibrary.com).

The exact mechanisms behind progression to castration resistance remain poorly understood. However, recent studies suggest that neuroendocrine (NE) cells, as well as pathways involving or bypassing the androgen receptor (AR), may play an important role in the development of castration resistance [3]. NE cells are present in both the normal and neoplastic prostate. They regulate surrounding prostate cells by secreting growth-modulating neuropeptides such as chromogranin A, serotonin and parathyroid hormone-related protein (PTHrP) [4]. Increases in the NE phenotype and secretory products are thought to be closely associated with progression and castration resistance in prostate cancer [5,6]. Previously, we developed an NE allograft (NE-10) and its cell line (NE-CS) from the prostate of the LPB-Tag 12T-10 transgenic mouse [7–9]. We demonstrated that secretions from NE cells induced androgen-independent growth of human prostate cancer cell line LNCaP and promoted pulmonary metastasis [10]. Therefore, it is crucial to seek a new drug or drug combinations targeting these prostatic NE carcinoma models (NE-10 and NE-CS).

Zoledronic acid (ZOL) is a nitrogen-containing bisphosphonate that inhibits bone resorption of osteoclasts through the inhibition of farnesyl-pyrophosphate synthetase in the mevalonate pathway. This agent has been demonstrated to have beneficial effects in patients with bone metastases of prostate cancer, reducing bone pain and skeletal-related events [11]. ZOL was also shown to have direct anti-tumor activity in several cancer cell lines. It is suggested that ZOL inhibits proliferation and induces apoptosis by impairment of prenylation of Ras and other small GTP-binding proteins (G proteins) [12].

Somatostatin is a peptide hormone that regulates secretion of various exocrine and endocrine glands via specific somatostatin receptors (SSTR). Five different subtypes (SSTR1-5), which are coupled to G proteins, have been identified [13]. Since a majority of NE tumors predominantly express SSTR2, somatostatin analogs having high affinity for SSTR2a such as octreotide (SMS) are considered to be drugs for NE tumors [14,15]. Since several studies have reported that SSTR1 and SSTR5 are expressed in addition to SSTR2 in prostate cancer tissue [15,16], new somatostatin analogs such as pasireotide (SOM) that have high affinity for SSTR5 in addition to SSTR2 [17], may be useful as new drugs for prostatic NE carcinoma.

In the present study, we investigated whether the growth of NE carcinoma models (NE-10, NE-CS) could be influenced by ZOL and/or somatostatin analogs (SMS and SOM), having potential anti-tumor activities.

MATERIALS AND METHODS

Cell Lines and Lell Culture

NE-CS is a murine prostate neuroendocrine cancer cell line established in our institute [9]. It was derived from an NE-10 tumor [8]. Passage numbers between 12, and 16 were used in the study. The NE-CS cells were maintained in the culture medium described below in 5% CO_2 in a humidified incubator. The medium consisted of RPMI-1640 (Gibco BRL, Breda, The Netherlands) that was supplemented with MEM nonessential amino acid (10 ml/L, Gibco BRL), MEM sodium pyruvate, penicillin–streptomycin (10 ml/L, Gibco BRL), 10% fetal bovine serum (FBS, ICN Biomedicals, Costa Mesa, CA), and 7.5% $NaHCO_3$.

ReverseTranscription Polymerase Chain Reaction (RT-PCR) Analysis

To investigate expression of SSTR in NE-10, RT-PCR analysis was performed. Tumor tissues in allografts of NE-10 were homogenized. Total RNA was extracted using an RNeasy kit (Qiagen, Valencia, CA) according to the manufacturer's instructions. A total of 2 μg of total RNA was reverse transcribed in a thermal cycles (Perkin–Elmer, Norwalk, CT) using SuperScript III (Invitrogen, Carlsbad, CA) and oligo (dT) 12–18 primers according to the manufacturer's instructions for 1 hr at 50°C in a 40 μl reaction mixture. Resulting cDNA (1 μl) was amplified with Taq polymerize and one set of oligonucleotide primers. Samples were denatured for 5 min at 94°C, and then amplified for 35 cycles at 94°C for 30 sec, 57°C for 30 sec, and 72°C for 1 min. Aliquots (9 μl) from each PCR sample were then analyzed by agarose-gel electrophoresis. Forward and reverse primer sequences were as follows: SSTR2a (5′-CAGCTGTACCATCAACTGGC, 5′-ATTTGTCCTGCTTACTGTCG), SSTR2b (5′-TGATCAATGTAGCTGTGTGG, 5′-CAAAGAACATTCTGGAAGC), SSTR5 (5′-TGCCTGATGGTCATGAGTGT, 5′-GGAAACTCTGGCGGAAGTTA), GAPDH (5′-TACAGCAACAGGGTGGTGGA, 5′-ACCACAGTCCATGCCATCAC).

Growth of NE-10 Allografts In Vivo

To examine the in vivo effects of ZOL, SMS and SOM as single agents and their combinatorial effects on prostatic NE carcinoma, we used NE-10 allografts. Six-week-old male BALB/c nude mice were castrated using the scrotal approach. After one week, 50 mg tissue fragments of the NE-10 allograft were inoculated subcutaneously (s.c.) into the flanks of mice. Two weeks after transplantation, NE-10 tumors grew to a volume of more than 100 mm^3. The mice were then

randomized into six treatment groups (13 mice in each group): ZOL, SMS, SOM, ZOL plus SMS, ZOL plus SOM, and control. The groups were treated for 6 weeks with ZOL (1 μg/mouse, three times per week, s.c.), SMS (2 μg/mouse, once per day, s.c.), SOM (2 μg/mouse, twice per day, s.c.), ZOL plus SMS (1 μg/mouse, three times per week, s.c. plus 2 μg/mouse, once per day, s.c.), ZOL plus SOM (1 μg/mouse, three times per week, s.c. plus 2 μg/mouse, twice per day, s.c.), or saline (an equal volume of solvent/day, s.c.). These substances were dissolved in 100 μl saline. ZOL, SMS, and SOM were kindly provided by Novartis Pharma AG (Basel, Switzerland). These agents were soluble in saline. The body weights of mice were measured each week. The effects of treatments on tumor growth were determined by measuring tumor volume (0.523 × long diameter^2 × short diameter). After 6 weeks of treatment, the mice were killed and the tumor and liver were removed. Liver weight was measured, and the numbers of metastatic nodules on the liver surface were macroscopically counted. The tissues were fixed in 10% formalin and embedded in paraffin. The 5 μm thick paraffin-embedded material was routinely processed for hematoxylin and eosin staining.

The Animal Experiment Committee of Sapporo Medical University approved the in vivo experiments. Animal care and housing followed the guidelines of the Animal Experiment Committee.

Cell Cycle and Apoptosis Analysis of Tissue Sections

Immunohistochemical staining was done with formalin-fixed paraffin-embedded tissue sections of NE-10 tumors. The 5 μm thick sections were deparaffinized in xylene and rehydrated in graded alcohol. Antigen retrieval was done by boiling sections for 20 min in a microwave oven in preheated 0.01 mol/L sodium citrate buffer (pH 6.0). Endogenous peroxidase activity was blocked by 3% hydrogen peroxide in ethanol for 10 min. After blocking with 1% non-fat dry milk in phosphate-buffered saline (PBS) (pH 7.4), the sections were reacted with a rabbit polyclonal anti-Ki-67 antibody (Abcam plc., Cambridge, UK) at 20 μg/ml or preimmune sera for 1 hr, followed by incubation with biotinylated goat anti-rabbit IgG (Nichirei, Tokyo, Japan) for 30 min. Subsequently, the sections were stained with streptavidin-biotin complex (Nichirei), followed by incubation with 3,3-diaminobenzidine and counterstaining with hematoxylin. The same tissues were immunostained by TdT-mediated dUTP-biotin nick-end labeling (TUNEL) (In situ Apoptosis Detection Kit, Takara Bio, Inc., Otsu, Japan). The Ki-67 labeling index (KI) and apoptotic index (AI) were determined as the ratios of immunohistochemically positive cells per 1,000 NE cells by using a fluorescence microscope (model BZ-9000; Keyence, Osaka, Japan).

Proliferation Assays

NE-CS cells (1 × 104) were suspended with 100 μl of culture medium in a 96-well plate for 24 hr, and then treated with the indicated concentrations (from 0.1 to 100 μmol/L) of ZOL, SMS and SOM for 24, 48, or 72 hr. For combination, the same concentrations of ZOL and SMS or SOM were used; for example, 1 μmol/L of ZOL to 1 μmol/L of SMS. In addition, they were treated with the indicated concentrations (from 0.1 to 100 μmol/L) of ZOL plus 1, 5, and 20 μmol/L of farnesyl-pyrophosphate ammonium salt (FOH) (Sigma–Aldrich, St. Louis, MO) for 48 hr. FOH is an isoprenoid to be involved in prenylation of several G proteins including Ras in the intracellular mevalonate pathway. Cell proliferation was assessed using a WST-8 (modified tetrazolium salt) cell proliferation kit (Cell Counting Kit-8, Dojin, Japan). Changes in absorbance at 450 nm were measured with a microplate reader. The growth inhibition was determined as the concentration inducing 50% inhibition (IC50). For analysis of the synergism between ZOL and somatostatin analogs (SMS and SOM), the combination indices (CI) were calculated by the isobologram equation method [18,19], and CI values of <1, 1, and >1 were considered to indicate synergistic, additive, and antagonistic effects, respectively 12.

Cell Cycle and Apoptosis Assays

NE-CS cells (3 × 104) were suspended with 100 μl of culture medium in a 96-well plate for 24 hr, and then treated with various concentrations of ZOL (from 10 to 100 μmol/L) for 48 hr. Then the cells were fixed with 4% paraformaldehyde, permeabilized with 0.1% Triton X-100, and labeled with the TUNEL technique (In situ Cell Death Detection Kit TMR red, Roche Diagnostics, Mannheim, Germany) and the primary anti-Ki-67 antibody at a 1/200 dilution (Abcam plc., Cambridge, UK). The Ki-67 antibody was detected with an Alexa Fluor 488 donkey anti-rabbit antibody, and nuclei were stained with 4,6-diamidino-2-phenylindole (DAPI) (Invitrogen, Carlsbad, CA). As in the in vivo study, the KI and the AI were measured by fluorescence immunohistochemistry using a fluorescence microscope (model BZ-9000; Keyence, Osaka, Japan).

Migration Assays

Cell migration analyses were performed as described previously (10). In a trans-well culture

chamber (Coster Science, Cambridge, MA), a polyvinylpyrrolidone-free polycarbonate filter with an 8.0 μm pore size was precoated with 5 μg of fibronectin (Biomedical Technologies, Stoughton, MA) on the lower surface. Two different experiments were performed. In experiment 1, NE-CS cells (1×10^5) were placed in the upper chamber with 100 μl of culture medium with or without ZOL (10, 100 μmol/L). In the lower chamber, 600 μl of culture medium was added. In experiment 2, NE-CS cells (1×10^5) were placed in the upper chamber with 100 μl of culture medium adding 20 μmol/L of FOH with or without ZOL (10, 100 μmol/L). In the lower chamber, 600 μl of culture medium was added. The cells that migrated across the pores at 2, 4, 6, and 8 hr were counted under a microscope after hematoxylin and eosin staining. The experiments were carried out in triplicate. Data are shown as number of cells 1 mm ^{2} of membrane.

Pull Down and Western Blot Assays

NE-CS cells (1×10^5) were suspended with 2 ml of culture medium in a 6-well plate for 24 hr, and then treated with ZOL (10, 100 μmol/L) or ZOL (10, 100 μmol/L) + 20 μmol/L FOH for 48 hr. Subsequent to the treatment, cells were washed three times with ice-cold PBS and solubilized in lysis buffer [RIPA buffer, 100 mmol/L PMSF, 500 mmol/L Na_3VO_4, 1 mol/L NaF, 2 mol/L Sigma 104 phosphatase substrate, Protease Inhibitor Mini Cocktail]. The total protein content of the cell lysates was determined by the BCA Protein Assay (Pierce, Rockford, IL).

Activated Ras was detected by pull-down assay. The GTP-bound form of Ras in the cell lysates was affinity-purified using the Raf1-Ras-binding domain (RBD)-GST complexed with glutathione beads following the manufacturer's instructions (Active Ras Pull Down and Detection Kit, Thermo Fisher Science, Waltham, MA). Complexes were analyzed by SDS–PAGE and immunobloting with a Ras-specific antibody.

The cells lysates obtained were boiled in SDS sample buffer containing 0.5 mol/L 2-mercaptoethanol. Samples were separated by SDS–PAGE, transferred to polyvinylidene difluoride (PVDF) membranes and immunoblotted with rabbit monoclonal anti-Erk1/2 and anti-phospho-Erk1/2 antibodies (Cell Signaling Technology Inc., MA), and a mouse monoclonal anti-β-actin antibody (Sigma–Aldrich). Separated proteins were visualized using horseradish peroxidase with enhancement by chemiluminescence (GE Healthcare Bio-Sciences Corp., NJ).

Statistical Analysis

We used the computer program StatView 5.0 for Windows (SAS Institute, Cary, NC). Student's *t*-test was applied to compare results between two different groups. Repeated-measures ANOVA was used when comparing the in vivo tumor volume, and the in vitro cell migration in an individual group. One-way ANOVA was used when comparing the in vivo apoptosis, cell cycle progression, and liver metastases in an individual group. Statistical significance was assigned at $P < 0.05$.

RESULTS

Expression of SSTR2a and SSTR5 in NE-10 Allografts

Since effects of somatostatin analogs are mediated by expression of SSTR, we examined expression of the somatostatin receptor subtypes SSTR2 and SSTR5, to which SMS and SOM preferentially bind, respectively. Gene expression of SSTR2a and SSTR5 was observed in NE-10 allografts, but that of SSTR2b was not (Fig. 1).

Effects of ZOL, SMS and SOM as Single Agents and in Combination on Subcutaneously Inoculated NE-10 Allografts

Growth of NE-10 tumors in mice treated with ZOL, ZOL plus SMS, and ZOL plus SOM was significantly slowed compared to the saline control ($P = 0.003$, $P < 0.001$, and $P = 0.001$, respectively) (Fig. 2A). All treatments were well tolerated with maintenance of body weight (data not shown). We examined whether anti-tumor effects of each treatment were induced by apoptosis or cell cycle arrest by using TUNEL and Ki67 staining, respectively (Fig. $2B_1$). The AI was significantly increased in tumors of mice treated with ZOL, ZOL plus SMS, or ZOL plus SOM compared to the control (means: 9.2, 11.6, and 12.7, respectively, vs. 2.4) (Fig. $2B_2$). The KI was significantly decreased in tumors of mice treated with ZOL, ZOL plus SMS, or ZOL plus SOM compared to the control (means: 5.3, 8.3, and 4.2, respectively, vs. 15.9) (Fig. $2B_3$). The

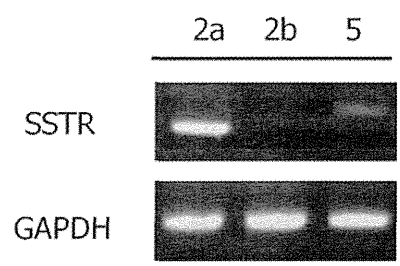

Fig. 1. Expression of SSTR2a, SSTR2b, and SSTR5 in NE 10 allograft by RT PCR. Gene expression of SSTR2a, and SSTR5 was observed in the NE 10 allograft, but that of SSTR2b was not.

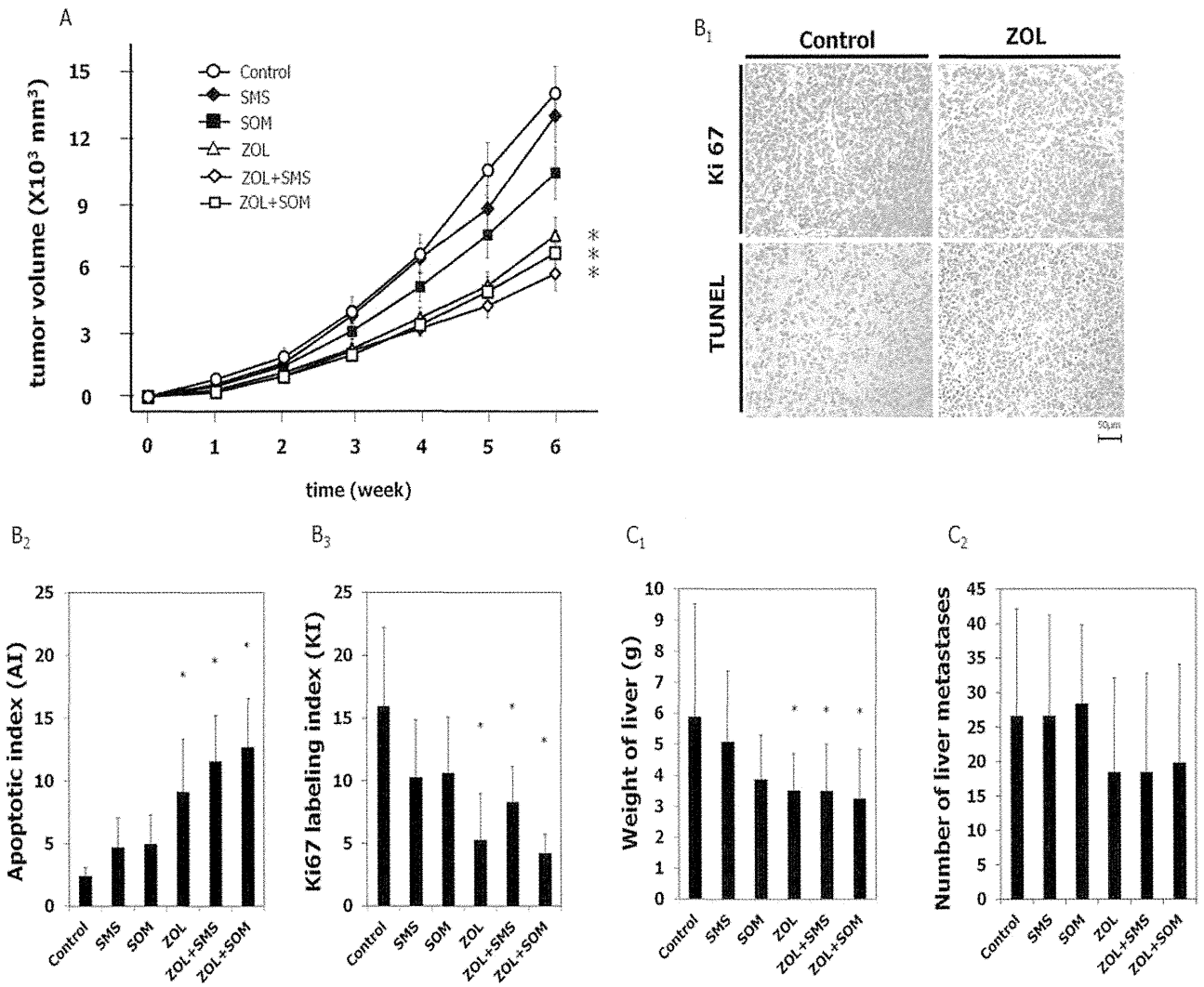

Fig. 2. Effects of ZOL, SMS, and SOM as single agents and in combination on subcutaneous inoculated NE 10 allografts. Six week old male BALB/c nude mice were castrated. After one week, 50 mg tissue fragments from the NE 10 allograft model were subcutaneously inoculated into the backs of mice. For 2 weeks, NE 10 tumors were allowed to grow to approximately more than 100 mm^3 before randomization into six treatment groups: control, ZOL, SMS, SOM, ZOL plus SMS, and ZOL plus SOM (n = 13/group). NE 10 allografts in each group were treated for 6 weeks. **A**: Growth of NE 10 tumors in mice treated with ZOL, ZOL plus SMS, and ZOL plus SOM was significantly slowed compared to the saline control ($P = 0.003$, $P < 0.001$, and $P = 0.001$, respectively). Data are means; bars ± SE; *, significantly different from control group ($P < 0.05$; repeated measures ANOVA). **B**: Effects of ZOL, SMS and SOM as single agents and in combination on apoptosis and cell cycle progression. Immunohistochemical staining was done by usingTUNEL and Ki67 staining (**B_1**). Apoptoic effects were measured by the number of TUNEL positive cells per 1,000 cells, apoptoic index (AI). The AI was significantly increased in tumors from mice treated with ZOL, ZOL plus SMS, or ZOL plus SOM compared to the control (means: 9.2, 11.6, and 12.7, respectively, vs. 2.4) (**B_2**). Cell cycle progression was measured by the number of Ki67 positive cells per 1,000 cells (KI: Ki 67 labeling index). The KI was significantly decreased in tumors from mice treated with ZOL, ZOL plus SMS, or ZOL plus SOM compared to the control (means: 5.3, 8.3, and 4.2, respectively, vs. 15.9) (**B_3**). Data are means; bars ± SD; *, significantly different from control group ($P < 0.05$; one way ANOVA). **C**: Effects of ZOL, SMS and SOM as single agents and in combination on liver metastases. The weights of livers having metastatic nodules in ZOL, ZOL plus SMS, or ZOL plus SOM were significantly lower than for the control (**C_1**). The numbers of metastatic nodules in these groups were not significantly different from the control (**C_2**). Data are means; bars ± SD. *, Significantly different from control group ($P < 0.05$; one way ANOVA).

weights of livers having metastatic nodules in ZOL, ZOL plus SMS, or ZOL plus SOM were significantly lower than for the control (Fig. $2C_1$), but the numbers of metastatic nodules in these groups were not significantly different from the control (Fig. $2C_2$).

Effects of ZOL, SMS and SOM as Single Agents and in Combination on Growth of NE-CS Cells In Vitro

We investigated the inhibitory effects of ZOL, SMS, and SOM, alone and in combination on proliferation

of NE-CS cells. Cell viability was measured by the WST-8 assay when NE-CS cells were treated with various concentrations of ZOL, SMS and SOM (0.1–100 μmol/L) in the treatment groups for 24, 48 or 72 hr. For combinations, the same concentrations of ZOL and SMS or SOM were used. The IC50 for ZOL at 72 hr was 15.7 μmol/L, whereas those for ZOL plus SMS, and ZOL plus SOM were 14.1, and 13.5 μmol/L, respectively (Fig. 3A). The combination of ZOL and somatostatin analogs did not demonstrate synergistic effects (CI: 0.57–1.00). ZOL induced time- and dose-dependent proliferative inhibition of NE-CS cells (Fig. 3B). These effects of ZOL were reversed by 20 μmol/L of FOH (Fig. 3C).

ZOL Inhibits Cell Cycle Activity and Induces Apoptosis of NE-CS Cells

TUNEL-positive cells, indicated in red, increased with increased concentrations of ZOL. On the other hand, Ki-67-positive cells, colored green, decreased (Fig. 4A). We also analyzed the AI and KI with ZOL

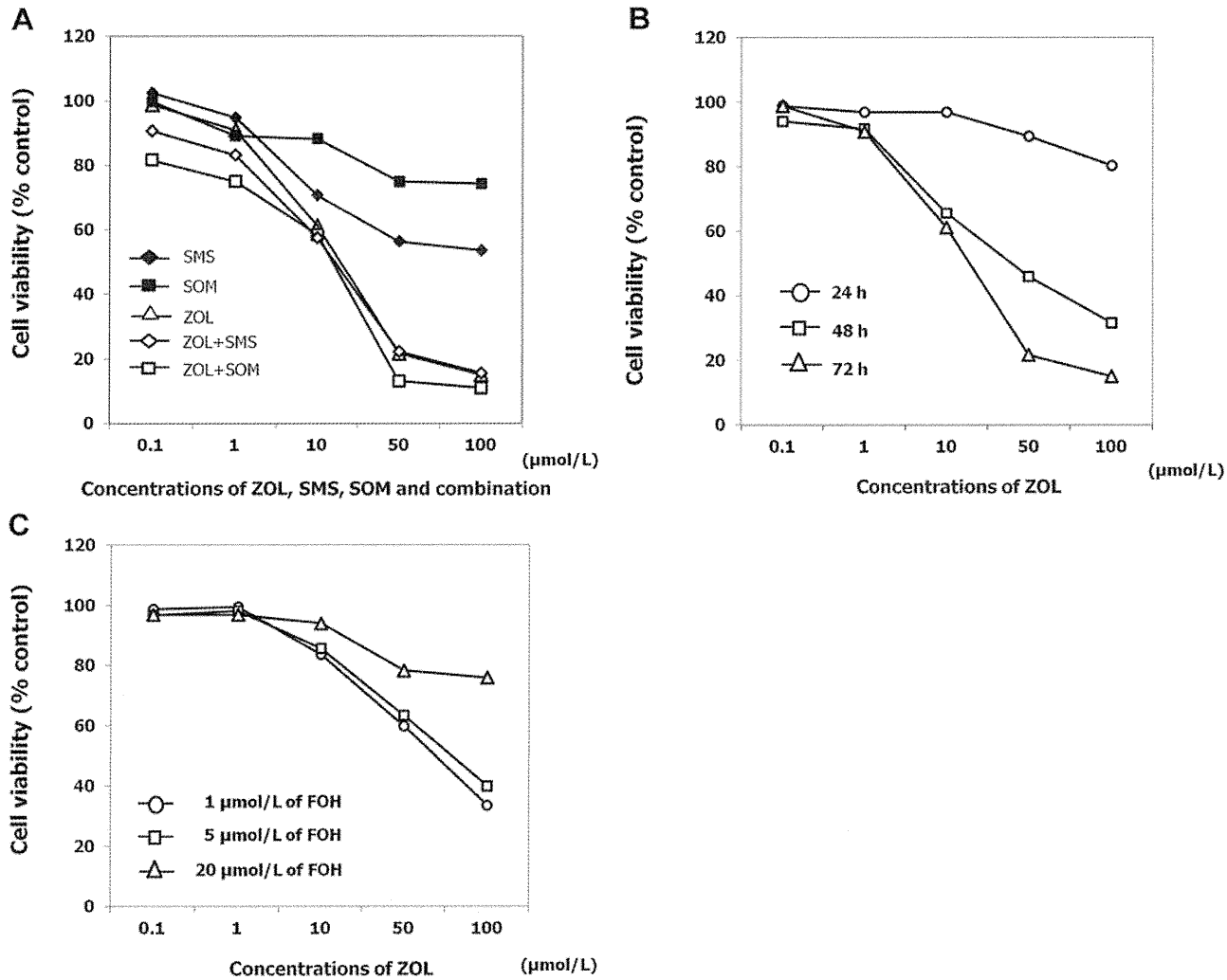

Fig. 3. Effects of ZOL, SMS and SOM as single agents and in combination on growth of NE CS cells. Cell viability was measured by WST 8 assay when NE CS cells were treated with various concentrations of ZOL, SMS and SOM (0.1–100 μmol/L) for 24, 48 or 72 hr. For combination, the same concentrations of ZOL and SMS or SOM were used. Cell viability was also measured when NE CS cells were treated for 48 hr with the indicated concentrations (from 0.1 to 100 μmol/L) of ZOL plus 1, 5, and 20 μmol/L of farnesyl pyrophosphate ammonium salt (FOH) (n = 5/group). **A**: Cell viability of NE CS cells at 72 hr in each treatment group. The IC50 of ZOL at 72 hr for NE CS cells was 15.7 μmol/L for ZOL, whereas it was 14.1 μmol/L for ZOL plus SMS, and 13.5 μmol/L for ZOL plus SOM. The combination of ZOL and somatostatin analogs did not create synergistic effects. **B**: Cell viability of NE CS cells in time and dose dependent manners. ZOL induced time and dose dependent proliferative inhibition of NE CS cells. **C**: Cell viability of NE CS cells at 48 hr in ZOL plus FOH. ZOL induced inhibition was reversed by 20 μmol/L of FOH.

concentrations of 0, 10, 50, and 100 μmol/L. The AI was significantly increased in ZOL 50, and 100 μmol/L compared to the control (means: 55.7 and 136.5, respectively, vs. 13.8) (Fig. 4B). The KI was significantly decreased in ZOL 10, 50, and 100 μmol/L compared to the control (means: 37.6, 22.8, and 1.3, respectively, vs. 68.7) (Fig. 4C).

ZOL Inhibits Migration of NE-CS Cells

In addition to effects of ZOL on cell cycle activity and apoptosis, we examined whether ZOL inhibited migration of NE-CS cells, using a Boyden chamber assay. NE-CS cells, with or without ZOL concentrations of 10, and 100 μmol/L, that migrated across the pores at 2, 4, 6 and 8 hr were counted. The numbers of cells migrating 1 mm ^{2} of membrane were significantly decreased in ZOL 10, and 100 μmol/L (Fig. 5A). When culture medium adding 20 μmol/L of FOH was incubated in upper chamber, the ZOL-induced inhibition was not appeared (Fig. 5B).

ZOL Utilizes the Ras/MAPK Pathway via the Mevalonate Pathway in NE-CS Cells

Since ZOL inhibits farnesyl-pyrophosphate synthetase in the mevalonate pathway and impairs prenylation of Ras, we evaluated the effects of ZOL on Ras activity. We used FOH, which potentially induces farnesylation of Ras. As evaluated by pull-down assay, 10, and 100 μmol/L inhibited Ras activation in NE-CS cells, and then the ZOL-induced inhibition was reversed by FOH (Fig. 6). We examined the effects of ZOL on Erk-1/2, which are the terminal proteins of the Ras/MAPK pathway. ZOL inhibited Erk1/2 phosphorylation as evaluated by Western blot assay.

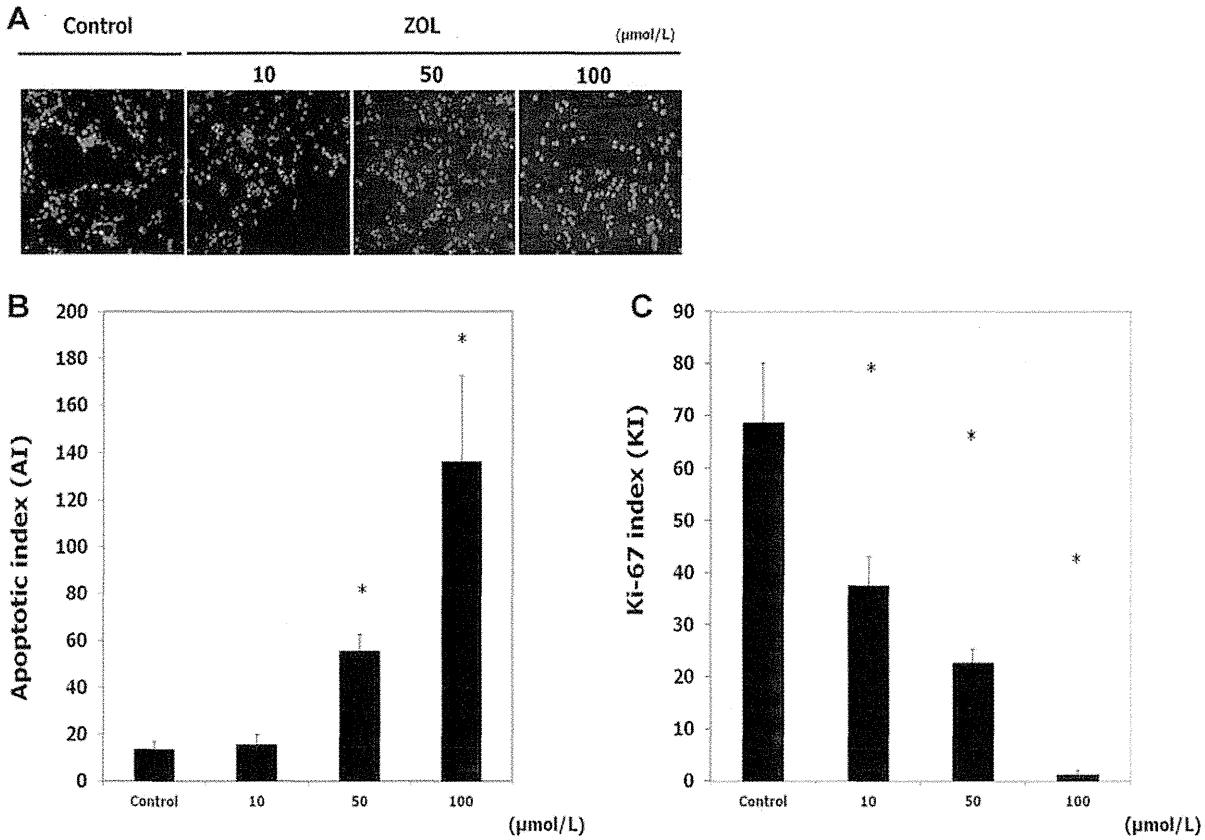

Fig. 4. Effects of ZOL on apoptosis and cell activity of NE CS cells. **A**: TUNEL and anti Ki67 immunofluorescence were used for NE CS cells treated with ZOL concentrations of 0, 10, 50, and 100 μmol/L (n = 5/group). DAPI was used to visualize cell nuclei. TUNEL positive cells, colored red, increased with increased concentrations of ZOL. On the other hand, Ki 67 positive cells, colored green, decreased. **B**: The numbers of TUNEL positive cells per 1,000 cells apoptoic index (AI) were significantly increased in ZOL 50, and 100 μmol/L compared to the control (means: 55.7, and 136.5, respectively, vs. 13.8). Data are means; bars ± SD; *, significantly different from control group ($P < 0.001$; Student's *t* test). **C**: The numbers of Ki67 positive cells per 1,000 cells (KI: Ki 67 labeling index) were significantly decreased in ZOL 10, 50, and 100 μmol/L compared to the control (means: 37.6, 22.8, and 1.3, respectively, vs. 68.7). Data are means; bars ± SD; *, significantly different from control group ($P < 0.001$; Student's *t* test).

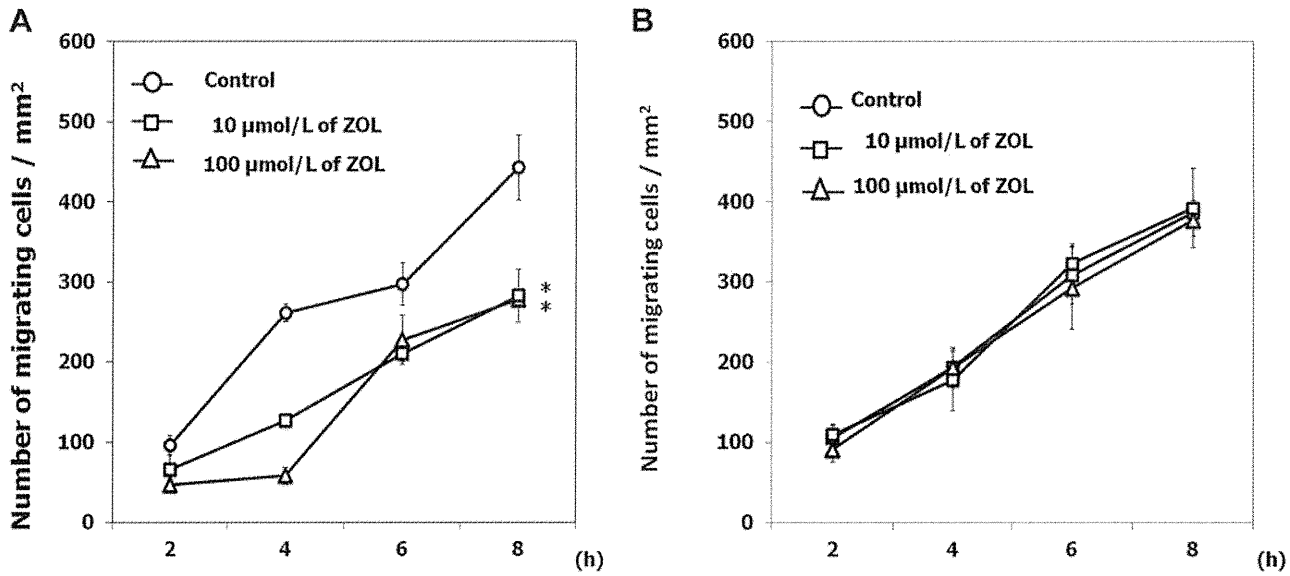

Fig. 5. Effects of ZOL on migration of NE CS cells. Migration assay was performed by using a Boyden chamber (n = 3/group). **A**: In experiment I, NE CS cells (1×10^5) were placed in the upper chamber with 100 μl of culture medium with or without ZOL (10, 100 μmol/L). In the lower chamber, 600 μl of culture medium was added. The numbers of cells migrating per 1 mm^{-2} of membrane were significantly decreased in ZOL 10, and 100 μmol/L. Data are means; bars ± SD; *, significantly different from the control ($P < 0.001$; repeated measures ANOVA). B: In experiment 2, culture medium adding 20 μmol/L of farnesyl pyrophosphate ammonium salt (FOH) was incubated in the upper chamber. The numbers of cells migrating 1 mm^{-2} of membrane were not significantly decreased in ZOL 10, and 100 μmol/L. Data are means; bars ± SD. *, Significantly different from the control ($P < 0.001$; repeated measures ANOVA).

DISCUSSION

Inappropriate NE regulation in the prostate might facilitate carcinogenesis, proliferation and other tissue changes such as loss of basal cells, angiogenesis, and piling up of prostatic luminal epithelium and invasion, which are characteristic of prostatic carcinoma [20]. In addition, we previously demonstrated that secretions from NE cells stimulated prostatic cancer cells to achieve androgen-independent growth [21]. Androgen deprivation therapy induces an increased number of NE cells in prostate cancer and the frequency and density of NE cells are more pronounced in CRPC [22]. Thus, the control of NE cells might be important for establishing a treatment strategy for CRPC.

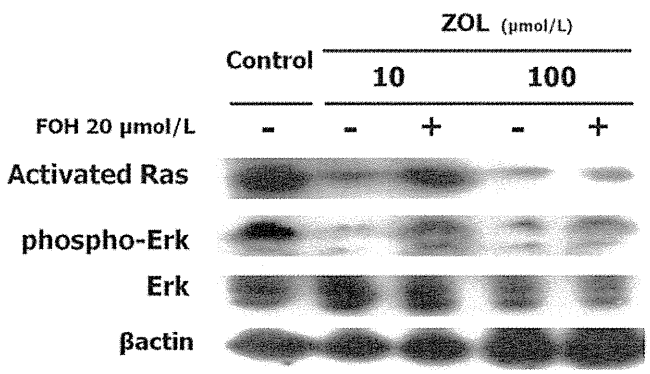

Fig. 6. Effects of ZOL on Ras/MAPK pathway of NE CS cells. We used farnesyl pyrophosphate ammonium salt (FOH), which potentially induces farnesylation of Ras. Ras activity was evaluated by pull down assay, and Erk activity by Western blot assay. As evaluated by pull down assay, 10, and 100 μmol/L ZOL inhibited Ras activation in NE CS cells, and then the ZOL induced inhibition was reversed by FOH. ZOL inhibited Erk1/2 phosphorylation in NE CS cells as evaluated by Western blot assay.

Somatostatin analogs have been used clinically used to treat NE tumors [23]. SMS and lanreotide, which have high affinity to SSTR2a, have been demonstrated to reduce excessive hormone production and accompanying symptoms from carcinoid tumors and pancreatic endocrine tumors such as glucagonoma, VIPoma and gastrinoma [14]. The anticancer effect may be the result of antiproliferative and apoptoic actions through direct and indirect mechanisms. The direct mechanism is mediated by SSTR on tumor cells, and suppression of secretion of several growth factors such as insulin-like growth factor-1 (IGF-1) may also indirectly inhibit the tumor growth [24–26]. In this study, in spite of the expression of SSTR2a and SSTR5 in our NE carcinoma models, we failed to find significant antiproliferative effects of SMS or SOM monotherapy in vitro or in vivo. In addition, the combination therapy with ZOL did not create a synergistic effect. Although, the exact reason is unclear, both

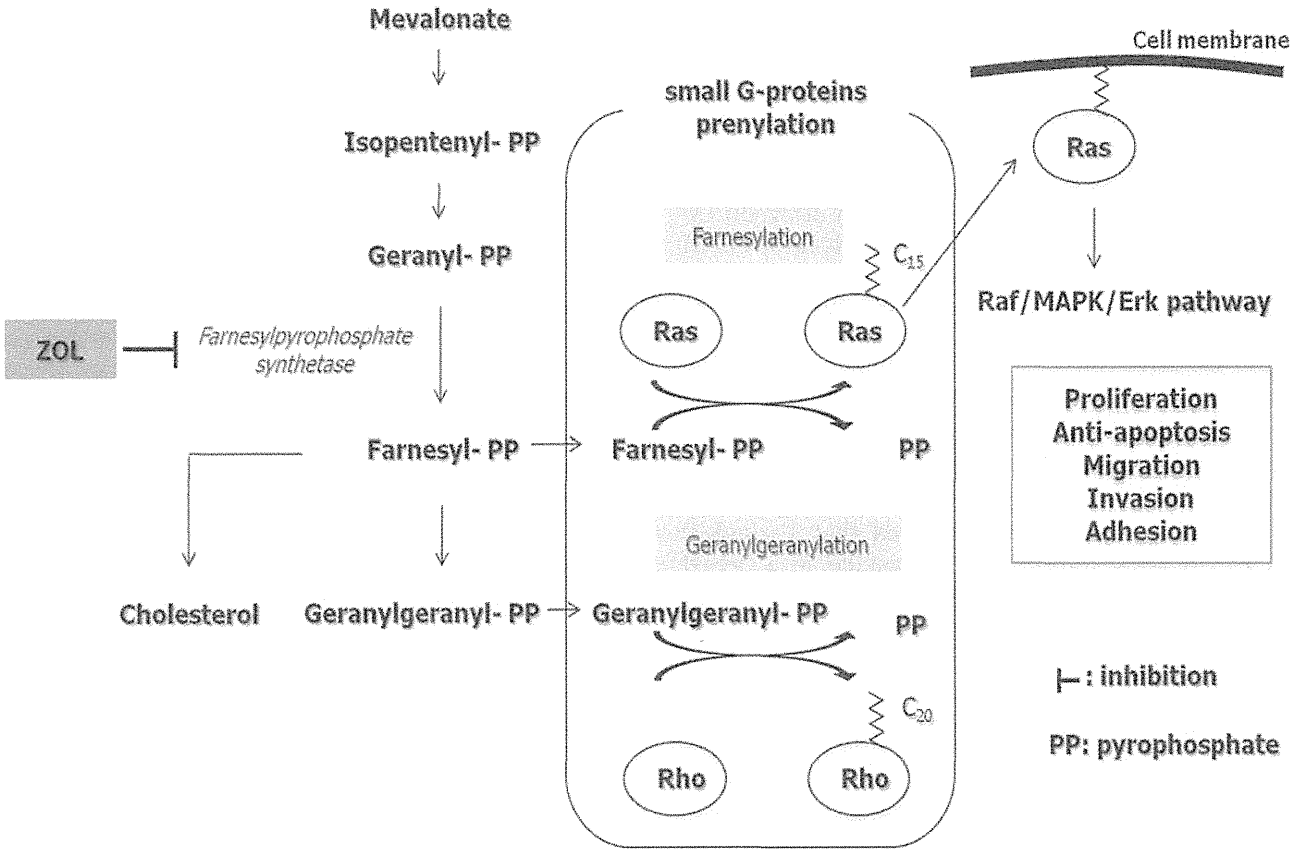

Fig. 7. Schematic representation of the mevalonate pathway and proposed mechanism of anti tumor effects of zoledronic acid in prostatic NE carcinoma.

SMS and SOM might be insufficient to control our NE carcinoma models through autocrine, paracrine and endocrine regulation via SSTRs.

Our results suggest that ZOL induces time- and dose-dependent antiproliferative and apoptoic effects in prostatic NE carcinoma. The observed anticancer activity was exerted at ZOL IC50 levels of from 15.8 to 36.0 μmol/L. In addition, the drug reduced migration by 8 hr in vitro even at the 10 μmol/L concentration, and the time and dose did not seem to affect the viability of cells. These effects were caused by disruption of prenylation of Ras proteins as a result of farnesyl-pyrophosphate synthetase inhibition, disrupting the downstream MAPK/Erk signaling pathway (Fig. 7). Farnesyl-pyrophosphate synthetase is a key enzyme in the mevalonate pathway, which produces essential lipid molecules such as cholesterol, farnesyl-pyrophosphate and geranylgeranyl-pyrophosphate [27]. Small G proteins need prenylation to link to the inner surface of the cell membrane and function in signal translation [28]. Prenylation of small G proteins involves farnesylation, which provides a 15-carbon isoprenoid moiety with Ras, and geranylgeranylation, which provides a 20-carbon isoprenoid moiety with Rap Rac or Rho [27,28]. Ras is the most thoroughly characterized member of the small G proteins involved in key oncogenic cellular processes such as proliferation, anti-apoptosis, migration, invasion and adhesion (Fig. 7). Therefore, it is anticipated that ZOL disturbing prenylation of Ras will induce multifactorial anticancer effects in cancer cells.

Several studies had shown that ZOL induces apoptosis via impaired prenylation of small G proteins in various cancer cells, including prostate [12,29–31], breast [32,33], myeloma [34], colon [35], and lung cancer cell lines [36]. Caraglia et al. [12] reported the effects of the combination of ZOL and farnesyl-transferase inhibitor R115777 on PC3 and DU145 prostate cancer cell lines. These effects paralleled disruption of Ras/MAPK/Erk and Akt survival pathways, which consequently decreased phosphorylation of both mitochondrial bcl-2 and bad proteins, and caspase activation. These findings may support our results indicating that ZOL induced apoptosis of NE cells. Recents studies have shown that impaired geranylgeranylation on other small G proteins such as Rap1 [29,34] and RhoA [32] is also crucial for the association with these apoptotic actions induced by ZOL.

We also demonstrated that ZOL induced cell cycle arrest of the NE carcinoma cells. Both in vitro, and in

vivo, ZOL reduced the numbers of Ki67-positive cells during all active phases of the cell cycle (G1, S, G2, and M). ZOL has been shown to reduce the expression of cyclin D1 and cyclin E in osteosarcoma cells, resulting in a cell cycle block at G1, and S [37]. In addition, experiments using leukemia cells have shown that ZOL can also reduce the expression of cyclin D3 and cyclin B, resulting in a cell cycle block at G2-M [38]. These actions are suggested to occur in a p53-independent manner followed by subsequent apoptosis. Our results indicated that ZOL inhibited the cell cycle of NE cells.

Moreover, we demonstrated that ZOL inhibited migration of NE-CS cells. It decreased the weights of livers having metastatic nodules in castrated NE-10 allografts, which means to suppress liver metastases. Likewise, Hiraga et al. [39] reported that 1 μmol/L ZOL significantly inhibited cell invasion in a breast cancer cell line (4T1/Luc), which consequently led to suppression of liver and bone metastases. Similar results were also observed in prostate cancer cell lines LNCaP, PC3, and DU145 31. In addition, Coxon et al. [40] reported an inhibitory effect of 1 μmol/L ZOL on adhesion to mineralized matrix in PC3, and DU145 cells. Although the exact mechanisms underlying these effects remain unclear, it is suggested that ZOL could inhibit several matrix metalloproteinase or adhesion molecules via impairment of prenylation of small G proteins. It is noteworthy that ZOL also inhibits essential steps for the spread of cancer cells. In addition, recent reports have shown that ZOL indirectly exerts anticancer effects via elevated function of gamma delta T cells [41,42]. It is suggested that accumulation of isopentenyl-pyrophosphate caused by ZOL may be involved in activation of gamma delta T cells [43].

There are some limitations in this study. The NE-10 allograft and the NE-CS cell line were derived from the mouse prostate. The role of human NE cells in human prostate cancer may be different from that of mouse NE cells. In addition, the characteristics of the established cell line, NE-CS, could be different from those of the original NE-10 allograft because cells suitable for survival in vitro were selected during establishment of the cell line. However, there are no ideal human lines for which both in vitro, and in vivo NE carcinoma models are available. In addition, the concentration of ZOL that induced anticancer effects in our experiments was high in comparison to the peak plasma levels (393 ± 100 ng/ml) usually achieved by intravenous infusion in patients [44]. Anticancer effects of ZOL might be considered to be exerted basically in bone metastatic lesions in which high concentrations of ZOL are achieved.

In patients with bone metastasis of prostate cancer, ZOL is commonly used for relieving pain and preventing skeletal-related events. This study revealed effects of ZOL on NE cells, potential triggers of prostate cancer leading to CRPC. Regulating the microenvironment between NE cells and prostate cancer cells may result in benefits to patients who do not have clinically detected bone metastasis. We believe that our results support the clinical rationale for earlier proactive use of ZOL, though further studies will be needed to confirm this.

CONCLUSION

We examined the in vitro, and in vivo anti-tumor effects of ZOL and somatostatin analogs (SMS and SOM) on NE carcinoma models. Our results indicate that ZOL, but not SMS or SOM, induces apoptosis and inhibition of proliferation and migration through impaired prenylation of Ras. Our findings support the possibility that ZOL could be used in the early phase for controlling NE cells which may trigger progression of prostate cancer to CRPC.

REFERENCES

1. Jemal A, Bray F, Center MM, Ferlay J, Ward E, Forman D. Global cancer statistics. CA Cancer J Clin 2011;61(2):69 90.
2. Heidenreich A, Aus G, Bolla M, Joniau S, Matveev VB, Schmid HP, Zattoni F. EAU guidelines on prostate cancer. Eur Urol 2008;53(1):68 80.
3. Debes JD, Tindall DJ. Mechanisms of androgen refractory pros tate cancer. N Engl J Med 2004;351(15):1488 1490.
4. di Sant'Agnese PA. Neuroendocrine differentiation in prostatic carcinoma: An update. Prostate Suppl 1998;8:74 79.
5. Ito T, Yamamoto S, Ohno Y, Namiki K, Aizawa T, Akiyama A, Tachibana M. Up regulation of neuroendocrine differentia tion in prostate cancer after androgen deprivation therapy, degree and androgen independence. Oncol Rep 2001;8(6): 1221 1224.
6. Hirano D, Okada Y, Minei S, Takimoto Y, Nemoto N. Neuro endocrine differentiation in hormone refractory prostate cancer following androgen deprivation therapy. Eur Urol 2004;45(5): 586 592; discussion 592.
7. Masumori N, Thomas TZ, Chaurand P, Case T, Paul M, Kasper S, Tsukamoto T, Shappell SB, Matusik RJ. A probasin Large T antigen transgenic mouse line develops prostate adenocarcino ma and neuroendocrine carcinoma with metastatic potential. Cancer Res 2001;61(5):2239 2249.
8. Masumori N, Tsuchiya K, Tu WH, Lee C, Kasper S, Tsukamoto T, Shappell SB, Matusik RJ. An allograft model of androgen independent prostatic neuroendocrine carcinoma derived from a large probasin promoter T antigen transgenic mouse line. J Urol 2004;171(1):439 442.
9. Uchida K, Masumori N, Takahashi A, Itoh N, Tsukamoto T. Characterization of prostatic neuroendocrine cell line estab lished from neuroendocrine carcinoma of transgenic mouse allograft model. Prostate 2005;62(1):40 48.

10. Uchida K, Masumori N, Takahashi A, Itoh N, Kato K, Matusik RJ, Tsukamoto T. Murine androgen independent neuroendo crine carcinoma promotes metastasis of human prostate cancer cell line LNCaP. Prostate 2006;66(5):536 545.
11. Saad F, Gleason DM, Murray R, Tchekmedyian S, Venner P, Lacombe L, Chin JL, Vinholes JJ, Goas JA, Chen B. A randomized, placebo controlled trial of zoledronic acid in patients with hormone refractory metastatic prostate carcino ma. J Natl Cancer Inst 2002;94(19):1458 1468.
12. Caraglia M, Marra M, Leonetti C, Meo G, D'Alessandro AM, Baldi A, Santini D, Tonini G, Bertieri R, Zupi G, Budillon A, Abbruzzese A. R115777 (Zarnestra)/Zoledronic acid (Zometa) cooperation on inhibition of prostate cancer proliferation is paralleled by Erk/Akt inactivation and reduced Bcl 2 and bad phosphorylation. J Cell Physiol 2007;211(2):533 543.
13. Patel YC. Somatostatin its receptor, family Front Neuroendoc rinol 1999;20(3):157 198.
14. Hejna M, Schmidinger M, Raderer M. The clinical role of so matostatin analogs as antineoplastic agents: Much ado about nothing? Ann Oncol 2002;13(5):653 668.
15. Reubi JC, Waser B, Schaer JC, Laissue JA. Somatostatin recep tor SSTR1 SSTR5 expression in normal and neoplastic human tissues using receptor autoradiography with subtype selective ligands. Eur J Nucl Med 2001;28(7):836 846.
16. Halmos G, Schally AV, Sun B, Davis R, Bostwick DG, Plonow ski A. High expression of somatostatin receptors and messen ger ribonucleic acid for its receptor subtypes in organ confined and locally advanced human prostate cancers. J Clin Endocri nol Metab 2000;85(7):2564 2571.
17. Bruns C, Lewis I, Briner U, Meno Tetang G, Weckbecker G. SO M230 a novel somatostatin peptidomimetic with broad so matotropin release inhibiting factor (SRIF) receptor binding and a unique antisecretory profile. Eur J Endocrinol 2002 ;146(5):707 716.
18. Chou TC, Talalay P. Quantitative analysis of dose effect rela tionships: The combined effects of multiple drugs or enzyme inhibitors. Adv Enzyme Regul 1984;22:27 55.
19. Topaly J, Zeller WJ, Fruehauf S. Synergistic activity of the new ABL specific tyrosine kinase inhibitor STI571 and chemothera peutic drugs on BCR ABL positive chronic myelogenous leu kemia cells. Leukemia 2001;15(3):342 347.
20. Bok RA, Small EJ. Bloodborne biomolecular markers in pros tate cancer development and progression. Nat Rev Cancer 2002;2(12):918 926.
21. Jin RJ, Wang Y, Masumori N, Ishii K, Tsukamoto T, Shappell SB, Hayward SW, Kasper S, Matusik RJ. NE 10 neuroendocrine cancer promotes the LNCaP xenograft growth in castrated mice. Cancer Res 2004;64(15):5489 5495.
22. Weinstein MH, Partin AW, Veltri RW, Epstein JI. Neuroendo crine differentiation in prostate cancer: Enhanced prediction of progression after radical prostatectomy. Hum Pathol 1996; 27(7):683 687.
23. Sciarra A, Bosman C, Monti G, Gentile V, Autran Gomez AM, Ciccariello M, Pastore A, Salvatori G, Fattore F, Di Silverio F. Somatostatin analogs and estrogens in the treatment of andro gen ablation refractory prostate adenocarcinoma. J Urol 2004;172(5 Pt 1):1775 1783.
24. Pawlikowski M, Melen Mucha G. Perspectives of new poten tial therapeutic applications of somatostatin analogs. Neuro Endocrinol Lett 2003;24(1 2):21 27.
25. van der Hoek J, van der Lelij AJ, Feelders RA, de Herder WW, Uitterlinden P, Poon KW, Boerlin V, Lewis I, Krahnke T, Hofland LJ, Lamberts SW. The somatostatin analogue SOM230, compared with octreotide, induces differential effects in several metabolic pathways in acromegalic patients. Clin Endocrinol (Oxf) 2005;63(2):176 184.
26. Schmid HA. Pasireotide (SOM230): Development, mechanism of action and potential applications. Mol Cell Endocrinol 2008;286(1 2):69 74.
27. Kavanagh KL, Guo K, Dunford JE, Wu X, Knapp S, Ebetino FH, Rogers MJ, Russell RG, Oppermann U. The molecular mechanism of nitrogen containing bisphosphonates as antios teoporosis drugs. Proc Natl Acad Sci USA 2006;103(20):7829 7834.
28. Hougland JL, Fierke CA. Getting a handle on protein prenyla tion. Nat Chem Biol 2009;5(4):197 198.
29. Nogawa M, Yuasa T, Kimura S, Kuroda J, Segawa H, Sato K, Yokota A, Koizumi M, Maekawa T. Zoledronic acid mediates Ras independent growth inhibition of prostate cancer cells. Oncol Res 2005;15(1):1 9.
30. Fabbri F, Brigliadori G, Carloni S, Ulivi P, Vannini I, Tesei A, Silvestrini R, Amadori D, Zoli W. Zoledronic acid increases docetaxel cytotoxicity through pMEK and Mcl 1 inhibition in a hormone sensitive prostate carcinoma cell line. J Transl Med 2008;6:43.
31. Mani J, Vallo S, Barth K, Makarevic J, Juengel E, Bartsch G, Wiesner C, Haferkamp A, Blaheta RA. Zoledronic acid influen ces growth, migration and invasive activity of prostate cancer cells in vitro. Prostate Cancer Prostatic Dis 2012;15(3):250 255.
32. Denoyelle C, Hong L, Vannier JP, Soria J, Soria C. New insights into the actions of bisphosphonate zoledronic acid in breast cancer cells by dual RhoA dependent and independent effects. Br J Cancer 2003;88(10):1631 1640.
33. Ottewell PD, Lefley DV, Cross SS, Evans CA, Coleman RE, Holen I. Sustained inhibition of tumor growth and prolonged survival following sequential administration of doxorubicin and zoledronic acid in a breast cancer model. Int J Cancer 2009;126(2):522 532.
34. Guenther A, Gordon S, Tiemann M, Burger R, Bakker F, Green JR, Baum W, Roelofs AJ, Rogers MJ, Gramatzki M. The bisphosphonate zoledronic acid has antimyeloma activity in vivo by inhibition of protein prenylation. Int J Cancer 2010;126(1):239 246.
35. Sewing L, Steinberg F, Schmidt H, Goke R. The bisphosphonate zoledronic acid inhibits the growth of HCT 116 colon carcino ma cells and induces tumor cell apoptosis. Apoptosis 2008; 13(6):782 789.
36. Tannehill Gregg SH, Levine AL, Nadella MV, Iguchi H, Rosol TJ. The effect of zoledronic acid and osteoprotegerin on growth of human lung cancer in the tibias of nude mice. Clin Exp Metast 2006;23(1):19 31.
37. Kubista B, Trieb K, Sevelda F, Toma C, Arrich F, Heffeter P, Elbling L, Sutterluty H, Scotlandi K, Kotz R, Micksche M, Berger W. Anticancer effects of zoledronic acid against human osteosarcoma cells. J Orthop Res 2006;24(6):1145 1152.
38. Kuroda J, Kimura S, Segawa H, Kobayashi Y, Yoshikawa T, Urasaki Y, Ueda T, Enjo F, Tokuda H, Ottmann OG, Maekawa T. The third generation bisphosphonate zoledronate synergisti cally augments the anti pH + leukemia activity of imatinib mesylate. Blood 2003;102(6):2229 2235.
39. Hiraga T, Williams PJ, Ueda A, Tamura D, Yoneda T. Zoledronic acid inhibits visceral metastases in the 4T1/Luc mouse breast cancer model. Clin Cancer Res 2004;10(13):4559 4567.